Full title:

Sex-Specific Ethylene Responses Drive Floral Sexual Plasticity in Cannabis

Short title:

Ethylene Drives Sexual Plasticity in Cannabis

Adrian S. Monthony[1,2,3,4], Julien Roy[1,2,3,4], Maxime de Ronne[1,2,3,4], Olivia Carlson[5], Susan J. Murch[5] & Davoud Torkamaneh[1,2,3,4*]

[1]Département de phytologie, Université Laval, Québec City, Québec, Canada

[2]Institut de Biologie Intégrative et des Systèmes (IBIS), Université Laval, Québec, Canada

[3]Centre de recherche et d'innovation sur les végétaux (CRIV), Université Laval, Québec, Canada

[4]Institut intelligence et données (IID), Université Laval, Québec, Canada

[5]Department of Chemistry, University of British Columbia, Kelowna, Canada

Monthony ORCID: 0000-0003-0536-691X

Roy ORCID: 0009-0002-9768-9096

de Ronne ORCID: 0000-0003-4062-3512

Murch ORCID: 0000-0001-5803-9483

*Torkamaneh ORCID: 0000-0002-9782-5695

*Corresponding Author

Email: davoud.torkamaneh.1@ulaval.ca

Abstract

Cannabis sativa L. exhibits remarkable sexual plasticity: both XX and XY individuals can undergo complete phenotypic sex reversal in response to ethylene modulation. While this phenomenon is well documented, the molecular mechanisms remain underexplored. Here, we present the first multi-omic study of hormonally induced sex change in both XX and XY *Cannabis* plants, integrating transcriptomic profiling, ethylene pathway metabolite quantification, and whole-genome sequencing across three genetically distinct genotypes. Treatments with silver thiosulfate (STS) and ethephon induced >80% phenotypic conversion, but transcriptomic responses diverged sharply between chromosomal sexes. We profiled 47 ethylene-related genes (ERGs) and identified 14 high-confidence candidates—including *CsACS1*, *CsACO5*, *CsERF1*, and *CsMTN*—with sex-specific, time-dependent expression patterns that support a two-phase model of plasticity: early transcriptional reprogramming followed by stabilization of new floral identities. Several candidate ERGs were in non-recombining regions of the X chromosome or absent from the Y, while most showed low nucleotide diversity, suggesting functional constraint. These findings provide a high-resolution view of ethylene-responsive sex plasticity and demonstrate that convergent floral phenotypes arise from distinct regulatory programs in XX and XY plants. Our work advances the molecular understanding of sexual plasticity in dioecious species and identifies candidate genes for the development of sex-stable cultivars in *Cannabis* and other crops.

Keywords: cannabis, sex determination, transcriptomics, multi-omics, sexual plasticity, ethylene, silver thiosulfate, ethephon

Introduction

Cannabis sativa L. (cannabis) is diploid species (2n=20) with nine autosomes and one pair of XX/XY sex chromosomes (Lapierre et al. 2023a; Monthony et al. 2024). Cannabis produces indeterminate compound inflorescences that develop distinctly dimorphic flowers: female flowers (FFs) consist of an ovary, surrounded by two bracts, dotted with glandular trichomes and two pistils (Reed 1914; Spitzer-Rimon et al. 2019), while male flowers (MFs) are staminate, characterized by a segmented perianth and five hanging stamen (Reed 1914). The glandular trichomes found on FFs synthesize medicinally important cannabinoids, of which over 100 have been characterized and are of interest for their potential medicinal applications (Giese et al. 2015; Mudge et al. 2019). In contrast, MFs produce cannabinoids at significantly lower levels and are considered to have negligible value in medicinal or commercial cannabis applications (Welling et al. 2021). Most drug-type cannabis is dioecious, producing exclusively male (XY) or female (XX) flowers, though some monoecious plants, mostly industrial hemp, produce both on the same plant (Ferfuia et al. 2021). Unlike most species, where the presence or absence of the Y chromosome alone determines sex, cannabis exhibits remarkable sexual plasticity—a plant's ability to alter its phenotypic sex in response to environmental or hormonal cues (Monthony et al. 2024). Under normal growth conditions the phenotypic sex of cannabis plants is concordant with sex chromosome karyotype. However, documented cases of hermaphroditism and monoecy have been reported to arise spontaneous and from human intervention (Kurtz et al. 2020; Punja and Holmes 2020). Although the cannabis genome has been sequenced and assembled (Grassa et al. 2021), and interest in sex determination is growing (Prentout et al. 2020; Adal et al. 2021; Shi et al. 2024b; Chen et al. 2025b; Orozco et al. 2025), the molecular pathways underlying sex expression remain poorly understood. Thus, understanding the genetic and hormonal regulation of flower development and sex determination in cannabis has significant implications for both basic plant biology and applied cultivation strategies.

Sexual plasticity, which has also been referred to as leaky, or labile sex expression (Käfer et al. 2022), has been described across diverse taxa of flowering monoecious and dioecious plants, including: *Carica papaya* (papaya; dioecious), *Spinacia oleracea* (spinach; dioecious), *Mercurialis annua* L. (monoecious) and *Amborella trichopoda* (dioecious; Komai and Masuda

53 2004; Sather et al. 2010; Lin et al. 2016; Anger et al. 2017; Cossard and Pannell 2021). However,
54 the triggers that shift phenotypic sex or floral sex ratios differ widely among species and
55 conditions, and include natural population variability (Anger et al. 2017), reproductive pressure
56 (Ji et al. 2016; Cossard and Pannell 2021), abiotic or biotic stressors (Lin et al. 2016), and targeted
57 molecular and plant growth regulator interventions (Thomas 2004; Zhang et al. 2017; García et al.
58 2020). Although the precise molecular mechanisms controlling sexual plasticity in cannabis
59 remain poorly understood, anecdotal reports from underground cultivators and subsequent
60 empirical validation by academic researchers strongly implicates ethylene biosynthesis and
61 signaling (Green 2005; Lubell and Brand 2018; Moon et al. 2020; Jones and Monthony 2022).
62 Known signaling inhibitors, such as silver thiosulfate (STS), reliably induce male flowers (IMFs)
63 in XX cannabis plants, while treatment with the ethylene-releasing compound ethephon
64 (commercially Ethrel®) consistently promotes female flower development (IFFs) in XY plants
65 (Lubell and Brand 2018; Moon et al. 2020; Flajšman et al. 2021). Similar roles for ethylene have
66 been demonstrated in the Cucurbitaceae family, where increases in endogenous ethylene or
67 exogenous applications result in an increased ratio of female to male flowers, resulting in ethylene
68 often being described as feminizing (Rajagopalan et al. 2004; Li et al. 2021). Research on
69 Cucurbitaceae has resulted in well-characterized gene networks involving ethylene biosynthesis
70 and signaling gene families, such as the ACC SYNTHASE (ACS), ACC OXIDASE (ACO), and
71 ETHYLENE RESPONSE (ETR; Boualem et al. 2015; Zhang et al. 2017; Li et al. 2021). In
72 *Cannabis*'s sister genus *Humulus* (hops), the dioecious species *H. lupulus* and *H. japonicus* also
73 exhibit ethylene-mediated sexual plasticity, with similar responses to STS and ethephon being
74 reported, but the molecular mechanisms underpinning this plasticity has not yet been elucidated
75 (Akagi et al. 2025). Beyond these examples, the regulatory pathways underpinning ethylene-
76 mediated sexual plasticity have not been widely studied, making the *C. sativa* a potentially
77 interesting dioecious analogue to Cucurbitaceae. Recently, our research group presented a first
78 integrative model of the ethylene precursor pathway, the Yang cycle (extensively review by Chen
79 et al. 2025a), as well as ethylene biosynthesis and signaling pathways in cannabis (Monthony et
80 al., 2024). This study generated an initial set of candidate ethylene-related genes (ERGs)
81 hypothesized to govern sexual plasticity, supported by preliminary transcriptomic evidence and
82 leveraging existing genetic datasets (Prentout et al. 2020; Adal et al. 2021). This model, as well as
83 most studies of cannabis sex to date, have focused on the role of ERGs in IMF production,

neglecting to consider whether XY feminization relies on reciprocal molecular and hormonal mechanisms.

Sexual plasticity is a complex, multi-layered process involving genetic, transcriptomic, hormonal, and metabolic networks. Previous transcriptomic studies, including those applying advanced inference methods like network ontology annotation (Orozco et al. 2025), have identified hormone-related gene expression changes associated with sexual plasticity and highlighted ethylene as an important regulator (Prentout et al. 2020; Adal et al. 2021). However, most research has primarily focused on sexual plasticity in XX plants and rarely explored reciprocal mechanisms in XY plants undergoing feminization, despite growing experimental evidence implicating ethylene as a central regulator of cannabis sex expression (Ram and Jaiswal 1970; Galoch 1978; Kurtz et al. 2020; Moon et al. 2020; Adal et al. 2021; Flajšman et al. 2021). Moreover, no previous studies have directly quantified ethylene-pathway metabolites in cannabis during sex transitions. Interpretation of these transcriptomic studies is further complicated by well-documented limitations of gene ontology (GO)-based methods, including incomplete annotations, inconsistent term specificity, and poor taxon representation—issues especially pronounced in non-model species like cannabis (Uygun et al. 2016; Gaudet and Dessimoz 2017; Fattel and Lawrence-Dill 2025). Another limitation of existing studies is the narrow focus on floral tissues during sex transition. This approach implicitly assumes that sex-determining signals arise only once flowers are visibly developing. However, in many plants species, key floral fate regulators—such as FLOWERING LOCUS T (FT)—are activated in leaves in response to photoperiod changes and then transported to the shoot apical meristem to trigger flowering (Tsuji 2017). Recently, evidence has emerged to support *C. sativa* following this conserved model, suggesting that *C. sativa* FT-like genes are responsive to photoperiod changes prior to the emergences of flowers (Dowling et al. 2024).

In this study, we apply multi-omic framework—integrating transcriptomic, metabolomic, and genomic data—to enable higher-resolution interrogation of temporally dynamic regulatory networks underlying sexual plasticity in cannabis. By analyzing both genotypic and pre-floral tissue variation, our study offers a more complete view of the ethylene-responsive signaling

114 networks coordinating sexual plasticity in cannabis. Our findings reveal that this process is not
115 governed by a single genetic switch but is instead a temporally dynamic process involving distinct
116 sets of genes. We identify genes likely involved in the initiation of sex change shortly after
117 treatment, as well as others that contribute to stabilizing the new phenotypic state. Together, these
118 results support a dynamic, phase-dependent model of ethylene-regulated sexual plasticity in
119 cannabis.

120 Results

121 Highly inducible sexual plasticity in XX and XY cannabis

122 The ability of cannabis to exhibit sexual plasticity was evaluated by quantifying the percentage of
123 flowers in the inflorescence whose phenotypic sex is opposite to the plant's chromosomal sex. A
124 two-way fixed effects analysis of variance (ANOVA) was performed to assess the effects of
125 treatment and genotype on the percentage of sex change, 28 days following the switch to a
126 flowering photoperiod (12/12). Treatment had a significant effect on the extent of sex change ($p <$
127 0.001), whereas genotype ($p = 0.07$) and the interaction between genotype and treatment ($p = 0.91$)
128 were not significant (Supplementary Table 9). Across all three genotypes, treated inflorescences
129 exhibited average sex change rate > 80% (Table 1). In contrast, H_2O treated control plants showed
130 no evidence of sexual plasticity in any genotype (Table 1). The observed phenotypic changes in
131 treated plants are visually presented in Figure 1 and Supplemental Figure 1.

132

133 **Table 1** Percentage of florets in *C. sativa* inflorescences that changed sex in response to sex
134 plasticity induction treatments. FF- female flowers; MF- male flowers; IFF- induced female
135 flowers; IMF- induced male flowers. Uncertainty indicated by standard error of the mean (SEM)
136 and differing letters indicate significant differences between treatments ($p \leq 0.05$), as determined
137 by a Tukey-Kramer post-hoc test.

Sex	Treatment	Genotype	Sex Change (%)
		Deadly Kernel	
XX	Control	La Rosca	0.0 ± 0.0^{a}
		Panama Pupil V4	

		Deadly Kernel	
XY	Control	La Rosca	0.0 ± 0.0[a]
		Panama Pupil V4	
		Deadly Kernel	96.3 ± 2.6[b]
XY	Treated (Ethephon)	La Rosca	89.0 ± 5.6[b]
		Panama Pupil V4	89.9 ± 4.0[b]
		Deadly Kernel	94.7 ± 1.0[b]
XX	Treated (STS)	La Rosca	92.5 ± 1.0[b]
		Panama Pupil V4	80.5 ± 5.0[b]

138

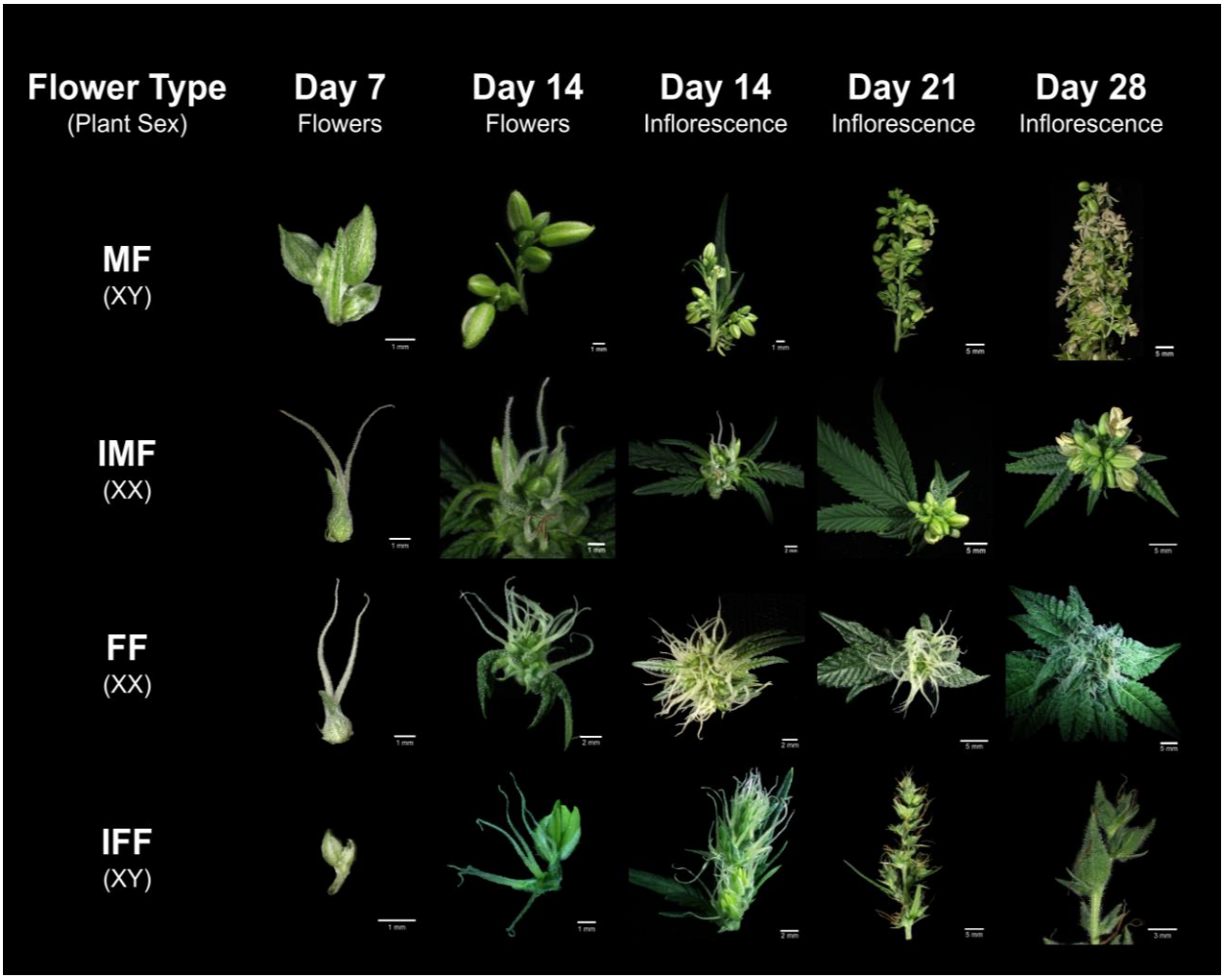

Figure 1 Representative timeline of floral development in MF, IMF, FF and IFF of *C. sativa* 'La Rosca' from 7 to 28 days after the photoperiod shift from long day to short day.

139

140 Cannabinoid analysis of control female flowers obtained from the three XX genotypes confirmed
141 THC-dominance (Chemotype I; Zheng 2022), with total THC content ranging from 16.98% to
142 25.40% w/w (Supplementary Table 10). Minor cannabinoids such as CBGA (0.28–1.20% w/w)
143 and CBG (0.04–0.12% w/w) were also detected at varying levels (Supplementary Table 10).

144 An updated ortholog identification reveals X-specific ERGs

145 An updated ortholog analysis identified six additional putative ERGs, expanding upon previous
146 findings (Monthony et al. 2024). This analysis utilized newly available *C. sativa* genomes,
147 including the new 'Pink Pepper' reference genome (NCBI 2023) and a fully phased X and Y-

148 haplotype genomes from a male Otto II genotype (Carey et al. 2024b). In total, 47 ERGs were
149 identified across the *C. sativa* genome (Supplementary Table 11), with the highest numbers found
150 on chromosomes 1 and X (Figure 2A).

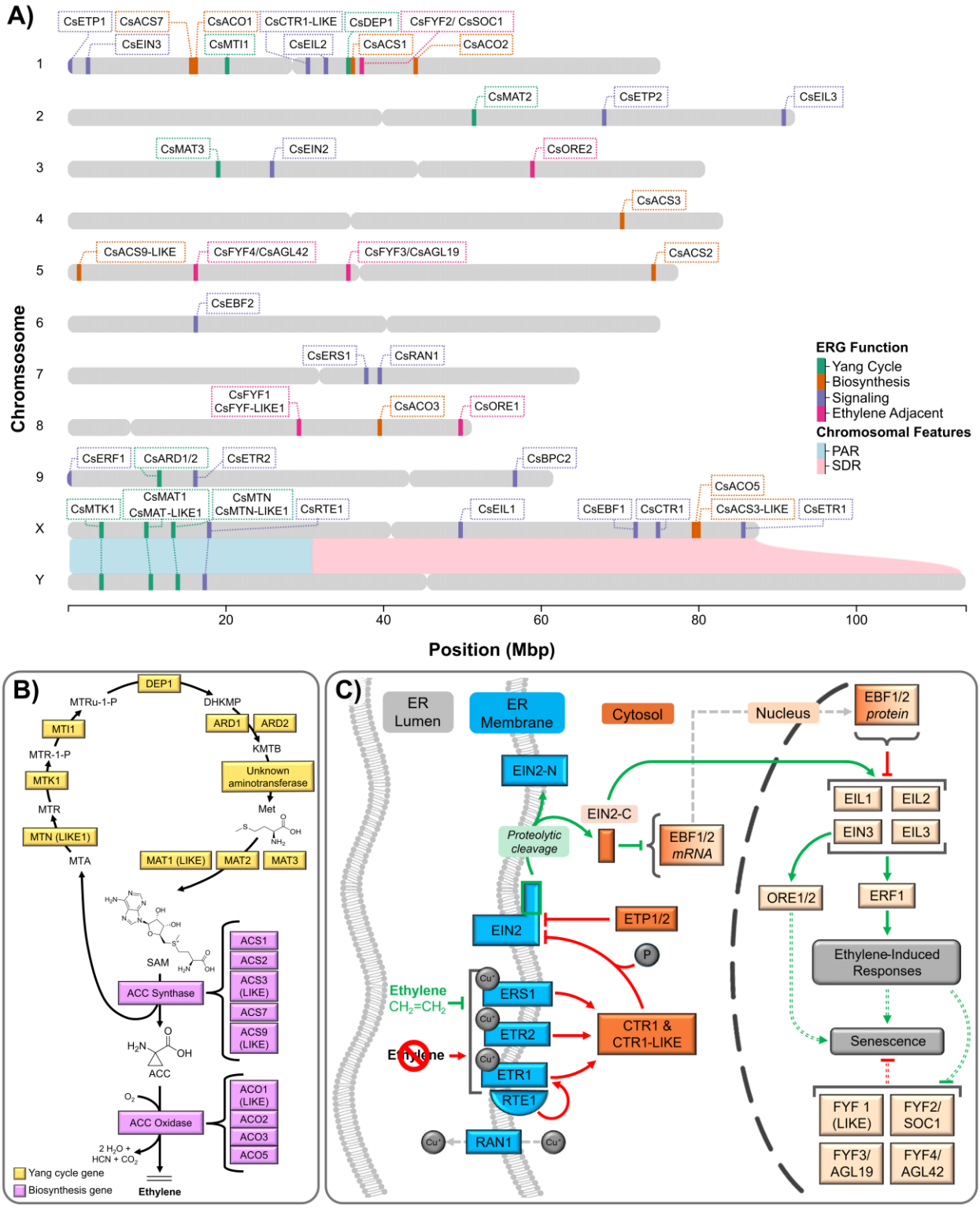
A)
CsETP1
CsACS7
CsACO1
CsCTR1-LIKE
CsDEP1
CsFYF2/ CsSOC1
CsEIN3
CsMTI1
CsEIL2
CsACS1
CsACO2
CsMAT2
CsETP2
CsEIL3
CsMAT3
CsEIN2
CsORE2
CsACS3
CsACS9-LIKE
CsFYF4/CsAGL42
CsFYF3/CsAGL19
CsACS2
CsEBF2
CsERS1
CsRAN1
CsFYF1
CsFYF-LIKE1
CsACO3
CsORE1
CsERF1
CsARD1/2
CsETR2
CsBPC2
CsACO5
CsMTK1
CsMAT1
CsMAT-LIKE1
CsMTN
CsMTN-LIKE1
CsRTE1
CsEIL1
CsEBF1
CsCTR1
CsACS3-LIKE
CsETR1
Chromosome
1
2
3
4
5
6
7
8
9
X
Y
20
40
60
80
100
Position (Mbp)
ERG Function
Yang Cycle
Biosynthesis
Signaling
Ethylene Adjacent
Chromosomal Features
PAR
SDR
B)
DEP1
MTRu-1-P
DHKMP
MTI1
ARD1
ARD2
MTR-1-P
KMTB
MTK1
Unknown aminotransferase
MTR
Met
MTN (LIKE1)
MTA
MAT1 (LIKE)
MAT2
MAT3
SAM
ACS1
ACS2
ACS3 (LIKE)
ACS7
ACS9 (LIKE)
ACC Synthase
ACC
ACO1 (LIKE)
ACO2
ACO3
ACO5
ACC Oxidase
2 H2O + HCN + CO2
Ethylene
Yang cycle gene
Biosynthesis gene
C)
ER Lumen
ER Membrane
Cytosol
Nucleus
EBF1/2 protein
EIN2-N
EIN2-C
EIL1
EIL2
EIN3
EIL3
Proteolytic cleavage
EBF1/2 mRNA
ORE1/2
ERF1
EIN2
ETP1/2
P
Ethylene-Induced Responses
Ethylene CH2=CH2
ERS1
ETR2
CTR1 & CTR1-LIKE
Ethylene
ETR1
RTE1
Senescence
RAN1
FYF 1 (LIKE)
FYF2/ SOC1
FYF3/ AGL19
FYF4/ AGL42

151

Figure 2 Updated genomic localization of ERGs and updated models of the ethylene pathway in *Cannabis sativa*. (A) Chromosomal positions of ethylene-related genes (ERGs) identified in *C. sativa* transcriptomes from Monthony et al. (2024) and expanded in the present study. Autosomal gene positions are based on the 'Pink Pepper' reference genome (NCBI, 2023); Pseudo-autosomal region (PAR) and non-recombining sex determination region (SDR) regions on the X and Y chromosomes follow Carey *et al.* (2024b). (B) Simplified model of the Yang cycle and ethylene biosynthesis pathway, updated from Monthony et al. (2024) to reflect gene presence in *C. sativa*. (C) Updated model of the canonical ethylene signaling pathway, including ER-localized receptors, CTR1-mediated EIN2 phosphorylation, and EIN2-C–dependent regulation of ethylene responses via EBF1/2, EIN3/EILs, ERF1, and FYFs. Color indicates subcellular localization (ER-bound: blue, cytosolic: orange, nuclear: light orange); arrowheads denote activation (pointed) or inhibition (blunt), in the presence (green) or absence (red) of ethylene. Dashed arrows indicating indirect or abbreviated steps. Single, grey dashed arrow indicates movement. A detailed review of ethylene biosynthesis and signaling pathways can be found in Binder (2020).

The newly available fully phased XY genome allowed us, for the first time, to report putative ERGs present in both the X and Y chromosomes, including those localized in the pseudoautosomal region (PAR) and the non-recombining sex-determination region (SDR; Figure 2A). Ortholog analysis identified six X-specific ERGs, all within the putative SDR region of the X chromosome. Additionally, four ERGs were detected in the X chromosome PAR, with homologs in the Y chromosome PAR. Notably, no Y-specific ERGs were identified. A complete list of genes present in the X and Y haplotypes of the Otto II genome can be found in Supplementary Table 11. Compared to our earlier analysis using the older cs10 genome assembly, which identified a single *MTN* gene, the improved ortholog resolution enabled by the Pink Pepper and Otto II genomes revealed two MTN-family genes. These were provisionally named *CsMTN* and *CsMTN-LIKE1*, based on sequence similarity to *Arabidopsis MTN1* and *MTN2*. *CsMTN* matched both *MTN1* and *MTN2*, while *CsMTN-LIKE1* showed weaker similarity to *MTN2* and had been annotated as a nucleosidase-like gene in the *C. sativa* reference genome (NCBI 2023; Supplementary Table 11). Taken together, these new ERGs were integrated into an updated model for the Yang cycle, ethylene biosynthesis and signaling (Figure 2 B &C).

Low nucleotide diversity suggests ERGs are highly conserved in *C. sativa*

To explore genetic variation within key CsERGs, we characterized single nucleotide polymorphisms (SNPs), structural variants (SVs), and nucleotide diversity (θ_π) across the whole

172 genome and 47 CsERGs. Variant calling on the genomes of XX and XY Deadly Kernel, La Rosca,
173 and Panama Pupil V4 (n = 6 genomes) identified approximately 6.7 million polymorphic SNPs
174 and ~78 thousand SVs relative to the *C. sativa* 'Pink Pepper' reference genome. Within ±5 kb
175 regions of the 47 CsERGs, 8,670 SNPs and 98 SVs were detected (Supplemental Figure 3A). Of
176 these, 3,611 SNPs and 29 SVs were located within CsERGs gene sequences and were further
177 examined for potential functional impact. The majority of variants were found in intronic regions
178 or the 3' and 5' UTRs, and were classified as having modifier impact (Supplemental Figure 3B&C).
179 Among coding region variants, most SNPs were synonymous, although 114 caused missense
180 mutations, and 13 high-impact variants (7 SNPs and 6 SVs) were identified (Supplemental Figure
181 3 D&E). Notably, LOC115719259 (*CsMAT2*), LOC115716986 (*CsFYF3*), and LOC115717309
182 (*CsFYF4*) exhibited a high density of SNPs, primarily within introns, consistent with their
183 predominantly (>90%) intronic gene structure. Additionally, LOC115706236 (*CsCTR1-LIKE*) and
184 LOC115702329 (*CsETR1*) also showed elevated SNP counts (>100 SNPs). Across these five
185 highly polymorphic genes, the average nucleotide diversity was 7.21×10^{-3}, notably higher than
186 the genome-wide average of 3.60×10^{-3} (Supplementary Table 12).

187

188 Across all CsERGs, the average nucleotide diversity was 2.85×10^{-3}, indicating lower diversity
189 than the genome-wide estimate. This signal was even more pronounced when excluding the five
190 highly polymorphic genes, with the remaining 42 CsERGs exhibiting an average nucleotide
191 diversity of 2.33×10^{-3}. Interestingly, CsERGs located in sex chromosome subregions also
192 displayed reduced variation: X-linked CsERGs within the SDR had an average nucleotide diversity
193 of 1.77×10^{-3}, while those located in the pseudoautosomal region (PAR) showed the lowest
194 diversity overall at 1.46×10^{-3}. The elevated SNP density observed in the five high-diversity genes
195 may reflect underlying structural variants miscategorized during alignment.

196

197 ACC Accumulation Differs by Sex and Stage

198 Endogenous ACC levels were quantified in *C. sativa* leaves at vegetative (day 0) and flowering
199 (day 1) stages across experimental groups (Supplemental Figure 4A and Supplementary Table 13).
200 Estimated marginal means from the linear mixed-effects model revealed that ACC concentrations

were significantly higher in XY Day 1 - IFF compared to XX Day 0 - FF and XX Day 1 - FF (Tukey's HSD, $\alpha = 0.05$). No other groups displayed significant differences in ACC levels. No significant change in ACC concentration was observed between pre- and post-flowering XY plants, regardless of treatment. Additionally, IMF exhibited intermediate ACC levels between male (XY) and female (XX) floral phenotypes. SAM quantification was below the level of quantification and is presented as presence/absence in Supplementary Table 13.

Among all ERGs analyzed, *CsCTR1-LIKE* expression exhibited a strong and significant negative correlation with ACC concentration in XX Day 0 - FF ($\rho = -0.8$, $p \leq 0.001$). However, no significant correlations were observed in other groups (Supplemental Figure 4B). Notably, all XY treatments exhibited weak positive correlations with *CsCTR1-LIKE* expression, suggesting a difference between *CsCTR1-LIKE* expression in XX and XY plants. Following STS treatment, IMF correlation remained strongly negative, while the control XX female flower exhibited only a weak correlation (Supplemental Figure 4B).

Transcriptomics and Network analysis

Time and sex-driven transcriptomic patterns in XX and XY plasticity

To understand the effect of sexual plasticity treatments on ERG expression over time and tissue-type, transcriptomes were obtained from leaves (day 0 and day 1) and immature flowers (day 14) across treated, and untreated XX and XY plants of the DK, LR and PP genotypes. This yielded 139 transcriptomes, comprising ~8 billion mapped reads with 24x coverage and high mapping quality (score = 103, insert size = 302 bp, Supplementary Table 8). PCA analysis found that the proportion of variance explained by the first two principal components increases over time (Figure 3A-C). At Day 0, PC1 and PC2 together account for 46.25% of the total variance (PC1: 29.07%, PC2: 17.18%). By Day 1, the combined variance explained increased to 61.94% (PC1: 41.66%, PC2: 20.28%), and at Day 14, it reached 74.05% (PC1: 49.41%, PC2: 24.64%). At day 0, PCA of ERG expression in untreated leaves showed a clear separation between XX and XY samples along PC1 (Figure 3A). The corresponding heatmap (Figure 3D) suggests that this clustering is driven

229 by a subset of highly expressed ERGs in XX plants, including *CsCTR1/CTR1-LIKE*, *CsMTK1*,
230 *CsFYF4/AGL42* and *CsACO3*.

231

232 Following photoperiod change and application of the sex-altering treatments, changes in ERG
233 expression patterns were observed at day 1. An increased variance is observed among treated
234 groups, notably ethephon-treated XY plants (IFF) which showed a sharp divergence from other
235 treatments along both principal components (Figure 3B). The heatmap for day 1 (Figure 3E)
236 highlights elevated expression of ethylene signaling genes in IFF plants, including *CsEBF1*,
237 *CsERS1*, *CsRTE1*, *CsETR2* and *CsEBF2*.

238

239 By day 14, PCA of ERG expression in immature flowers reveals a partial overlap between IFFs
240 and the FF controls tissues (Figure 3C). The heatmap (Figure 3F) shows two distinct blocks of
241 floral organ concordant (FOC) gene expression –shared gene expression among flowers of the
242 same phenotypic sex. A female-biased, FOC block of ERGs including genes from the Yang Cycle
243 (*CsMAT2/3*, *CsMTK1* and *CsDEP1*), ethylene biosynthesis (*CsACS2* and *CsACS3-LIKE*) as well
244 as ethylene signaling and signaling-adjacent genes (*CsFYF2, CsFYF4* and *CsCTR1-LIKE*) are
245 clustered in the top rows (Figure 3F).

246

247 In contrast, male expression patterns were more complex. PCA indicated that MFs and IMFs
248 remained distinct, with separation along both principal components (Figure 3C). The heatmap
249 (Figure 3F) revealed both FOC gene expression and the presence of uniquely expressed ERGs
250 (uERGs) in MFs. Male-biased ERGs included *CsMTN/MTN-LIKE1* (Yang Cycle), *CsACS1*,
251 *CsACS7*, *CsACO5* (biosynthesis), and multiple ethylene signaling-related genes (*CsEBF1,*
252 *CsEBF2, CsERF1, CsFYF3, CsRAN1, CsEIN3, CsEIN2, CsBPC2*). Additionally, a set of uERGs
253 was highly expressed only in MFs, including *CsARD2, CsMTI1, CsMAT1* (Yang Cycle), *CsACO2,*
254 *CsACO1* (biosynthesis), and *CsETP1, CsETR2, CsORE1, CsORE2* (signaling).

255

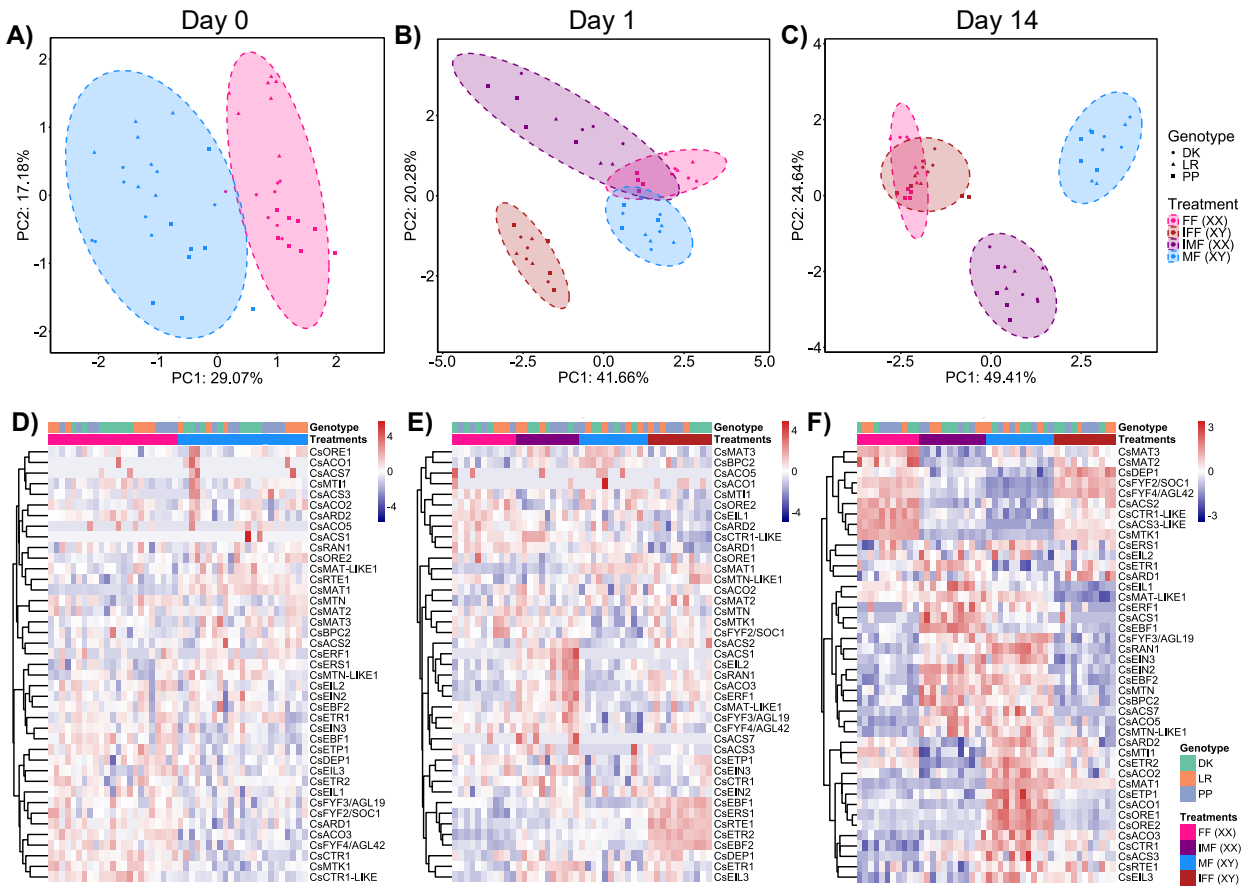

Figure 3 Principal Component Analysis (PCA) and heatmaps of 47 ERG expression across experimental time points and treatments. PCA was performed on batch-corrected variance-stabilized transformed (VST) counts of 47 ERGs. (A) Day 0 (pre-treatment, leaves); (B) Day 1 (post-treatment, leaves); (C) Day 14 (post-treatment, immature flowers). Each point represents an individual sample, and ellipses indicate the 95% confidence intervals for each group. Colors correspond to treatment groups, while symbols indicate cultivars (DK: Deadly Kernel, LR: La Rosca; PP: Panama Pupil V4). D-F) Heatmaps displaying expression patterns of 47 ERGs for each time point. Heatmap colors represent z-scores of gene expression, with rows corresponding to genes and columns to samples. The hierarchical clustering of genes (y-axis) was performed using Euclidean distance and complete linkage.

Network analyses reveal XX and XY-unique ERGs involved in sexual plasticity

The PCA suggesting distinct XX and XY ERG expression patterns in response to sexual plasticity treatments led us to construct two separate sex-specific gene co-expression networks. This allowed for the identification of modules specific to each genotypic sex without cross-sex effects influencing module detection. WGCNA network construction for XX and XY plants resulted in networks with 12 and 16 module Eigengenes (ME), respectively. Hierarchical clustering

263 dendrograms (Supplemental Figure 5A & B) display the gene co-expression relationships within
264 these sex-specific networks. Distinct clustering patterns and variations in module compositions,
265 size and number were observed between the XX and XY networks.

266

267 Module-trait correlation analyses were performed independently for the XX and XY networks to
268 identify modules significantly associated with treatment and specific time points (Supplemental
269 Figure 5C & D). Priority was given to modules strongly correlated with treatment to identify gene
270 clusters most responsive to the experimental conditions. In the XX network (Supplemental Figure
271 5C), five modules displayed significant correlations with treatment: MEbrown (r = -0.89),
272 MEblack (r = -0.52), MEmagenta (r = 0.54), MEblue (r = 0.66) and MEred (r = 0.71). For the XY
273 network (Supplemental Figure 5D), three modules surpassed the threshold for significant
274 correlation with treatment: MEgrey (r = 0.53), MEpink (r = 0.65), and MEgreenyellow (r = 0.5).

275

276 From these treatment-associated modules, ERGs were extracted for further investigation,
277 identifying 19 ERGs in the XX network, and 6 ERGs in the XY network, resulting in a total of 24
278 unique ERGs (Supplementary Table 13 and Supplementary Table 14). To evaluate their functional
279 significance within each module, intramodular connectivity (kME) was calculated. The most
280 highly connected gene in the XX network was *CsACO5* (kME = 0.96), while in the XY network,
281 *CsERF1* exhibited the highest connectivity (kME = 0.93). Interestingly, *CsERF1* was the only
282 gene present in both networks, with a kME of 0.95 in the XX network. All 24 ERGs were retained
283 for subsequent differential gene expression analysis.

284

285 **Differential expression analysis reveals 14 candidate sexual plasticity ERGs**

286 To refine the candidate ERGs involved in sexual plasticity, we conducted differential gene
287 expression (DGE) analysis on the 24 ERGs identified from treatment correlated XX and XY
288 WGCNA modules. Contrasts were set between treated and untreated samples of the same
289 genotypic sex at time points following sexual plasticity treatment (Day 1 and Day 14), and genes
290 were considered significantly differentially expressed if $|\log_2(\text{Fold Change})| \geq 1$ and adjusted p-
291 value ≤ 0.05 across all three genotypes. Of the initial 24 ERGs, 14 met these filtering criteria (grey

292 highlighted genes in Supplemental Figure 2). The resulting refinements yielded a candidate ERG
293 list including those most likely to play a role in ethylene-mediated sexual plasticity in *C. sativa*
294 (Table 2).

295

296 **Table 2** Candidate sexual plasticity ERGs in XX and XY *C. sativa*. Candidate ERG filtration
297 included those identified with a significant WGCNA correlation between module and treatment (r
298 ≥ 0.5; p-adjust ≤ 0.05) followed by a filtration using differential gene expression (DGE). DGE was
299 conducted intra-sex on day 1 or day 14 retaining only those genes which were significantly (p-
300 adjust ≤ 0.05) differentially expressed across all 3 tested genotypes. Log_2FC values denoted by a
301 * meeting filtration criteria for significant differential expression (p-adjust ≤ 0.05; $|log_2FC \geq 1|$; in
302 3 genotypes).

Sex Association	**CsERG**	**Locus ID (LOC)**	**Pathway**	**Intramodular Connectivity (kME)**		**Differential Expression (log_2FC)**			
						IMF (XX) vs. FF (XX)		**IFF (XY) vs MF (XY)**	
				XX Network	**XY Network**	Day 1	Day 14	Day 1	Day 14
XX/XY	*MTN*‡	115704327	Yang Cycle	0.73	0.67	0.02	1.14*	0.27	-1.01*
	MTN-LIKE1‡	133033195	Yang Cycle	0.79	0.73	-0.07	1.17*	0.20	-1.10*
	ACO3	115699412	Biosynthesis	-0.77	0.81	2.48*	0.27	1.68*	-0.61
	EBF1†	115720532	Signaling	-0.83	-0.63	0.22	1.56*	1.71*	-0.21
	FYF2/SOC1	115706939	Adjacent	-0.83	-0.95	-0.13	-1.22*	0.24	2.60*
	FYF4/AGL42	115717309	Adjacent	-0.82	-0.78	0.06	-1.69*	0.10	3.93*
XX	*MTK1*‡	115703014	Yang Cycle	-0.74	0.28	-0.01	-1.47*	0.32	0.90
	MAT2	115719259	Yang Cycle	0.81	0.48	0.12	-2.48*	0.11	0.38
	ACS1	115704849	Biosynthesis	0.94	0.38	6.03*	1.90*	0.17	-0.35
	ACS2	115717044	Biosynthesis	-0.47	-0.43	0.56	-1.72*	1.30*	0.82
	ACO5†	115699408	Biosynthesis	0.96	0.92	-0.23	4.17*	-0.01	-1.77
	ERF1	115723050	Signaling	0.95	0.93	5.37*	0.44	1.40	-1.20

XY	*EBF2*	115724585	Signaling	0.73	0.61	0.43	0.65	1.33*	-0.63
	RTE1‡	115707134	Signaling	0.65	0.73	0.05	0.03	1.50*	-0.10

† indicates that the gene is present only on the X chromosome

‡ indicates a gene is present on the X and Y chromosome

303

304 From the 14 candidate ERGs, six met the criteria for association with sexual plasticity in both XX
305 and XY sex changed plants, a further six were associated with XX plants only and two with XY
306 plants (Table 2). Within the XX and XX/XY-associated ERGs, there was representation from all
307 pathways including: Yang cycle (e.g., *MTN*, *MAT2*), ethylene biosynthesis (e.g., *ACS1*, *ACO5*),
308 signaling (e.g., *EBF1*, *ERF1*), and signaling adjacent regulatory pathways (e.g., *FYF4/AGL42*). In
309 contrast, the XY-associated ERGs were primarily limited to signaling components (*EBF2*, and
310 *RTE1*), perhaps reflecting the signaling response from the ethephon-induced sex change.

311

312 To identify temporal patterns underlying ethylene-induced sexual plasticity, we examined the
313 differential expression of ethylene-related genes (ERGs) at two stages: in mature leaves
314 immediately following treatment and photoperiod change (day 1) and in immature inflorescences
315 during active sexual phenotype transition (day 14). Genes strongly associated with day 1 by
316 WGCNA and/or differential expression analysis were classified as plasticity initiators, while those
317 associated with day 14 were classified as plasticity stabilizers (Figure 4).

318

319 In XX plants, three differentially expressed ERGs were significantly associated with plasticity
320 initiation and ten associated plasticity stabilization (Table 2). Initiators included *ERF1* ($\log_2$FC =
321 5.37) and *ACO3* ($\log_2$FC = 2.48; Figure 4A), which were significantly upregulated in IMFs
322 compared to FFs at day 1, suggesting early activation of ethylene biosynthesis and signaling
323 pathways. By day 14, several ERGs displayed substantial differential expression, including strong
324 upregulation of *ACO5* ($\log_2$FC = 4.17; Figure 4B) and *EBF1* ($\log_2$FC = 1.56), as well as moderate
325 upregulation of the Yang cycle-associated genes *MTN* ($\log_2$FC = 1.14; Figure 4B) and *MTN-LIKE1*
326 ($\log_2$FC = 1.17). In contrast, *MAT2* exhibited marked downregulation ($\log_2$FC = –2.48). *ACS1* was
327 the only ERG significantly differentially expressed at both timepoints in XX plants, with strong

upregulation at day 1 ($log_2FC = 6.03$) and sustained, though reduced, expression at day 14 ($log_2FC = 1.90$), suggesting a role in both the initiation and stabilization of sexual plasticity (Figure 4C).

In XY plants, five ERGs were classified as initiators and four as stabilizers (Table 2). Two initiators, *EBF2* ($log_2FC = 1.33$) and *RTE1* ($log_2FC = 1.50$), were differentially expressed only in masculinized XY plants and did not show corresponding changes in XX plants. Among stabilizers, *FYF2* and *FYF4* were strongly upregulated during the phenotypic transition observed at day 14 ($log_2FC = 2.60$ and 3.93, respectively). *MTN* and *MTN-LIKE1*, which were upregulated in XX plants, were downregulated in XY plants ($log_2FC = -1.01$ and -1.10, respectively; Figure 4B).

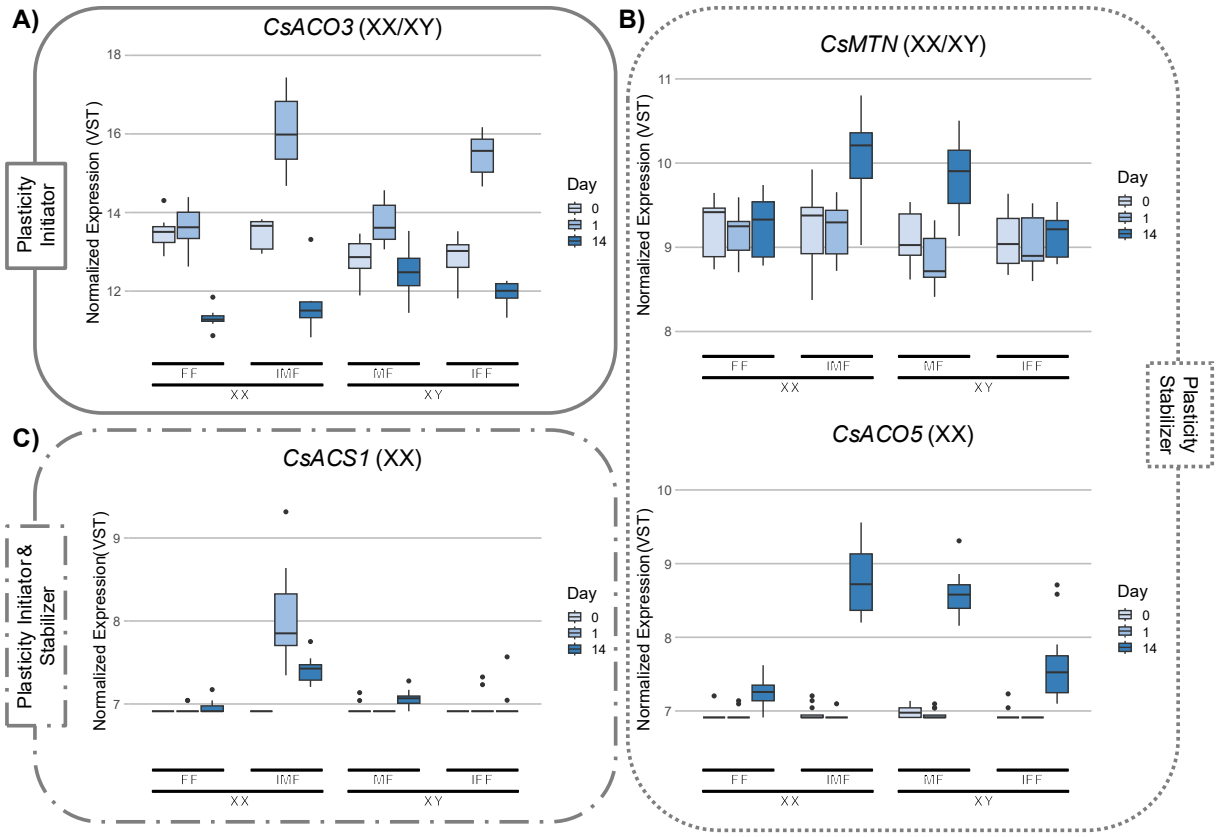

Figure 4 Representative VST normalized ERG RNA expression profiles for sexual plasticity initiators (A & C) and plasticity stabilizer genes (B), as identified using WGCNA and DGE filtration. Brackets next to names indicate chromosomal sex of plants where a significant effect of the gene on plasticity was identified.

339 The candidate ERGs were used to create a working model for the temporal control of ethylene-
340 regulated sexual plasticity (Figure 5). This model incorporates plasticity initiators and plasticity
341 stabilizers, highlighting their dynamic changes in sex- and treatment-specific expression profiles
342 over time. Importantly, candidate ERGs critical to sexual plasticity regulation appear consistently
343 at pathway bottlenecks, where alternate signaling routes are absent or limited. Key examples
344 include *MTN* and *MTK1* at the initiation of the Yang cycle, *ACS1/2* and *ACO3/5* in the
345 biosynthesis pathway (Figure 2B & Figure 5), and *EBF1/2* and *ERF1* in downstream signaling
346 (Figure 2C & Figure 5).

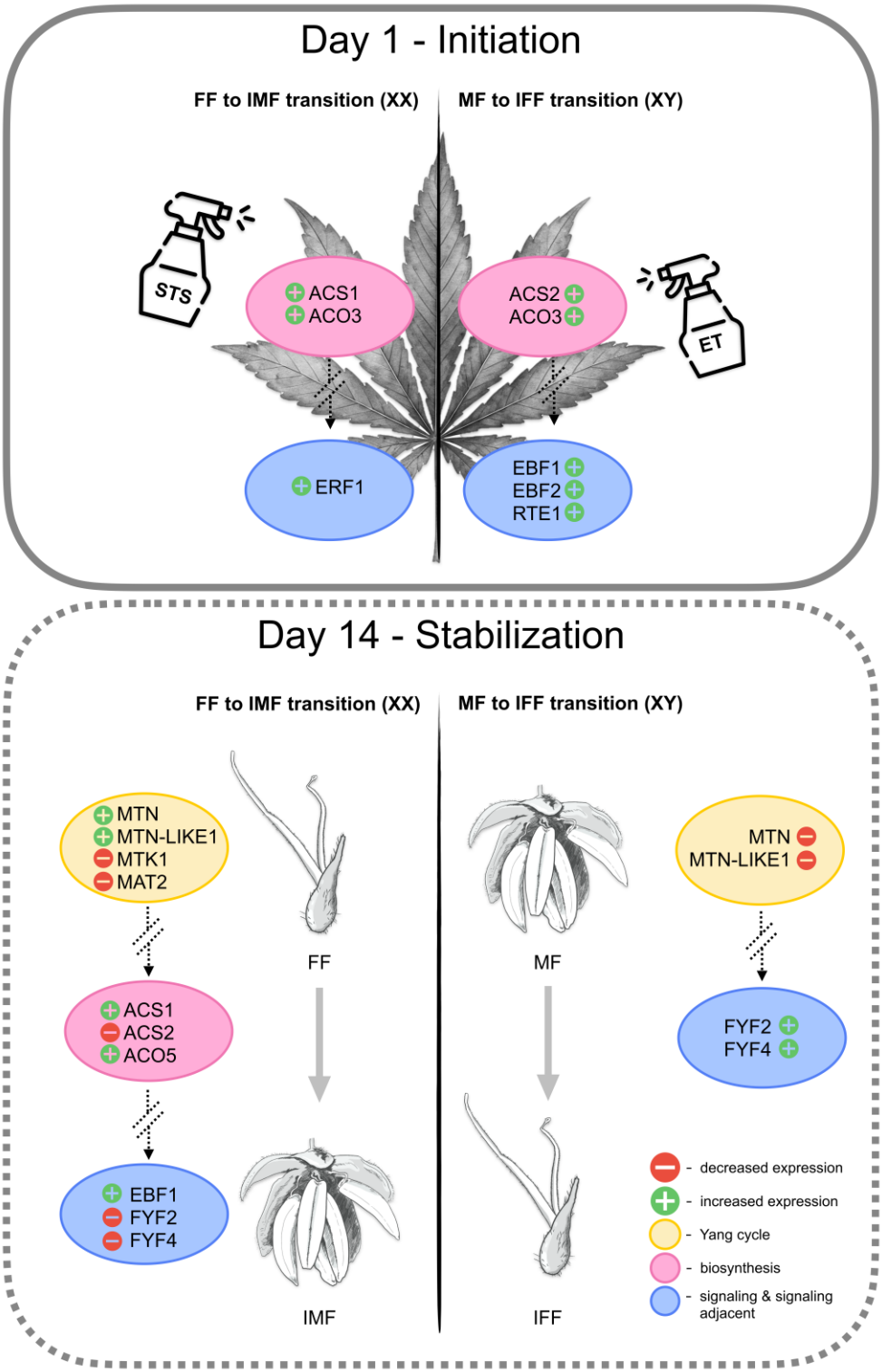
Day 1 - Initiation
FF to IMF transition (XX)
MF to IFF transition (XY)
STS
ACS1
ACO3
ACS2
ACO3
ET
ERF1
EBF1
EBF2
RTE1
Day 14 - Stabilization
FF to IMF transition (XX)
MF to IFF transition (XY)
MTN
MTN-LIKE1
MTK1
MAT2
FF
ACS1
ACS2
ACO5
EBF1
FYF2
FYF4
IMF
MF
MTN
MTN-LIKE1
FYF2
FYF4
IFF
- decreased expression
- increased expression
- Yang cycle
- biosynthesis
- signaling & signaling adjacent

347

Figure 5 Working model of ethylene-induced sexual plasticity in *C. sativa*. The model outlines two phases: initiation, marked by broad upregulation of ethylene biosynthesis and signaling genes in both IMFs (XX) and IFFs (XY); and stabilization, when ERG expression diverges between IMF and IFF plants. Key expression changes span the Yang cycle, biosynthesis, signaling, and adjacent pathways, and are shown as directional symbols (green "+" for upregulation, red "–" for downregulation) based on $\log_2$FC relative to untreated controls. FF→IMF and MF→IFF transitions reflect contrasts with untreated FFs and MFs, respectively. Flower illustrations by Alexandra K. McGregor.

Discussion

Ethylene-induced sexual plasticity is a dynamic, sex-specific process

Sexual plasticity, the capacity of a plant to shift its phenotypic sex from its baseline genetic sex in response to internal or external cues, is a phenomenon observed in many monoecious and dioecious species (Lin et al. 2016; Cossard and Pannell 2021; Käfer et al. 2022). In *Cannabis sativa*, there is long-standing experimental and anecdotal evidence supporting ethylene as a central regulator of this process (Galoch 1978; Moon et al. 2020; Adal et al. 2021). In this study, application of sex-altering treatments (silver thiosulfate for XX plants and ethephon for XY plants) reliably triggered phenotypic sex change in >80% of treated plants, confirming a conserved, inducible plasticity response (Table 1), achieving inflorescence sex change rates comparable to previous reports (Lubell & Brand, 2018; Moon et al., 2020).

Despite these shared phenotypic outcomes, our results reveal that XX and XY plants respond to ethylene modulation through distinct transcriptional programs. Analysis of 47 ethylene-related genes (ERGs) across time and tissue type uncovered a temporally dynamic, sex-specific response pattern, supporting a two-phase model of plasticity: (1) an early initiation phase, where shared upregulation of biosynthesis genes occurs shortly after treatment alongside divergent patterns of expression of ethylene signaling genes, and (2) a later stabilization phase, in which ERG expression diverges and consolidates new phenotypic sex identities (Figure 3; Figure 5). In the following sections, we explore how sex chromosome structure and gene location shape these responses, and how specific ERGs act as candidate regulators of each plasticity phase.

Plasticity initiation: ERG responses shortly after sex-change induction

Ethylene biosynthesis and signaling are the two gene families that make up the early responsive ERGs. Of particular interest are the biosynthesis genes *CsACS1* and *CsACS2*, which encode ACC synthase, and *CsACO3*, which encodes ACC oxidase—together catalyzing the two-step conversion of SAM to ethylene (Binder 2020). *CsACS1* was strongly upregulated in STS-treated XX plants (IMFs) at Day 1 ($\log_2$FC = 6.03) and remained elevated at Day 14 ($\log_2$FC = 1.90), indicating a potential dual role in initiating and stabilizing masculinization (Figure 5 & Table 2). Normalized expression data showed a sharp spike in *CsACS1* expression at Day 1 in IMFs (Figure 4C), accompanied by a modest increase in ACC concentration (Supplemental Figure 4), supporting its role as a plasticity-associated ethylene biosynthesis gene. Across all other tissues and treatments, including MFs and IFFs, *CsACS1* remained minimally expressed. In contrast, *CsACS2* displayed a broader and less clearly sex- or treatment-specific pattern. In XY plants, *CsACS2* was upregulated following ethephon treatment at Day 1 ($\log_2$FC = 1.30) and downregulated in IMFs by Day 14 ($\log_2$FC = –1.72), reaching levels similar to MFs. However, the magnitude of these changes was comparatively small. Normalized expression showed that *CsACS2* expression was distributed across multiple tissue types and timepoints, including elevated expression in IFFs and Day 1 MFs—suggesting a more constitutive role in ethylene production. Previous studies have reported similarly variable *CsACS2* expression. Our previous study of ERGs found higher *CsACS2* expression in FFs compared with IMFs and MFs (Monthony et al. 2024), while Borin *et al.* (2024) found no significant expression differences across FF, MF, and IMF flower tissues at Day 14 using qRT-PCR. These conflicting results may reflect tissue-type, developmental stage, or genotype-specific variation rather than a direct role in sexual plasticity. In other plant species, such as cucurbits and tomato, members of the ACS gene family show tissue- and stage-specific expression, with functionally distinct roles despite similar enzymatic activity (Van de Poel et al. 2014; Boualem et al. 2015). *CsACS2* may follow a similar pattern in *C. sativa*, highlighting the need for finer-resolution temporal and tissue-specific analyses to clarify its function.

CsACO3 was also differentially expressed in leaf tissues one day after sex-change induction, showing significant upregulation in both IMFs and IFFs ($\log_2$FC = 2.48 and 1.68, respectively;

400 Table 2). Although the magnitude of change was greater in XX plants, the consistent direction
401 across both sexes suggests *CsACO3* may serve as a shared ethylene biosynthesis initiator during
402 early reprogramming. This pattern aligns with its expected enzymatic function and may reflect a
403 transient upregulation to support immediate ethylene flux following hormonal induction. Further
404 exploration of its expression in floral tissues and later timepoints would help determine whether
405 *CsACO3* has a continued or transient role in sexual plasticity. Interestingly, our previous study of
406 ERGs in *C. sativa* sexual plasticity using flower tissues from MF, FF, and IMF plants (Monthony
407 et al. 2024) found that *CsACO3* expression was highest in MFs and lowest in FFs and IMFs,
408 suggesting a karyotype-concordant pattern of expression. In the current dataset, we again observe
409 highest expression in MFs at Day 14, with IFFs showing comparable levels—further validating
410 this karyotype-linked trend (Figure 4A). This study newly implicates *CsACO3* in early
411 reprogramming, underscoring its dynamic, stage-specific expression.

412

413 Despite the sharp transcriptomic induction of *CsACS1* and *CsACS2* following sex-change
414 treatments, this response was not fully mirrored in the measured ACC concentrations. For
415 example, despite substantial upregulation of *CsACS1* ($\log_2$FC = 6.03) in leaves of the IMF
416 treatment relative to FFs, the ACC levels remained similar between these groups (Supplemental
417 Figure 4). In contrast, IFFs exhibited the highest ACC concentration of all groups, despite a more
418 modest *CsACS2* induction ($\log_2$FC = 1.30), which more closely aligns with the anticipated
419 relationship between gene induction and metabolite output. This apparent disconnect between *ACS*
420 expression and *ACC* accumulation is consistent with previous findings in tomato, where tissues
421 producing the most ethylene—such as the pericarp—had relatively low ACC content and ACS
422 activity, while abundant *ACC* transcript levels were observed in tissues with limited ethylene
423 production (Van de Poel et al. 2014). These discrepancies have been interpreted as evidence for
424 tight spatial and temporal regulation of ACC metabolism and transport, as well as the rapid
425 conversion of ACC to ethylene in actively ripening or differentiating tissues. Possible explanations
426 for the elevated ACC levels observed in IFFs may reflect a lag between biosynthetic induction and
427 ACC turnover, a localized ethylene amplification loop triggered by exogenous ethephon, or even
428 the accumulation of ACC as a metabolic reserve—potentially stockpiled for future ethylene
429 biosynthesis depending on tissue-specific developmental cues. Together, these findings highlight

that ACC concentrations alone are insufficient indicators of ethylene biosynthetic activity, particularly during rapid transcriptional reprogramming. This underscores the complex interplay of transcriptional regulation, enzyme kinetics, and tissue-specific flux. Clarifying the roles of *CsACS1* and *CsACS2* in ethylene production will likely require future studies incorporating spatial transcriptomics and enzyme activity assays.

ERF1, a central transcriptional activator in the ethylene signaling pathway, acts downstream of *EIN3* and *EIL1* to mediate broad ethylene responses through direct activation of GCC-box-containing target genes (Solano et al. 1998; Binder 2020). Given the well documented role of ethylene response factors (ERFs) in ethylene-mediated developmental programming, and the recent association of *CsERF106* with sexual plasticity (Orozco et al. 2025), *CsERF1* is a plausible candidate for ethylene mediated sexual plasticity. In our dataset, *CsERF1* was strongly upregulated in STS-treated XX plants at Day 1 (IMFs vs FFs; $\log_2$FC = 5.37) and exhibited the highest kME values of all candidate genes in both the XX (0.95) and XY (0.93) WGCNA networks, indicating tight integration with other genes responsive to sex change treatments. Although the IFF vs MF contrast in XY plants showed a $\log_2$FC of 1.40, this effect did not meet our criteria for statistical significance due to genotype-level variability (Supplemental Figure 2). Nevertheless, this trend suggests that *CsERF1* may be responsive to ethylene exposure across both sexes, with a potentially conserved role in reprogramming floral identity. Taken together, these findings support a role for *CsERF1* as an early transcriptional integrator in ethylene-mediated sexual plasticity, particularly in XX plants, with evidence for broader involvement that warrants further investigation.

Plasticity stabilization: Genes consolidating new sexual identity

CsACO5, an X-linked gene with no Y copy, emerged as a compelling candidate for the stabilization of male floral identity during sexual plasticity, based on its strong and consistent upregulation in IMFs. Despite being X-linked, *CsACO5* levels are nearly identical in XY MFs and XX IMFs by Day 14, implying regulation by the male-flower program, not chromosome count (Figure 4B). Similarly, *CsACO5* expression in IFFs resembled that of FFs, with both groups exhibiting lower transcript levels. This floral organ concordant (FOC) expression pattern—where

459 gene expression reflects phenotypic sex rather than chromosomal sex—is consistent with Borin *et*
460 *al*. (2024) and Monthony *et al*. (2024), both of whom reported elevated *CsACO5* expression in
461 IMFs compared to FFs. At Day 14, *CsACO5* expression was markedly upregulated in IMFs
462 relative to untreated FFs ($\log_2$FC = 4.17), while normalized expression in MFs was comparable to
463 IMFs, and IFFs exhibited reduced expression levels similar to FFs, though with genotype-
464 dependent variability (Supplemental Figure 2E). *CsACO5* remains low at Day 0 and Day 1 in all
465 groups (Figure 4B).

466

467 Complementing this late-stage induction, another gene that may contribute to the stabilization of
468 male floral identity is *CsACS1*, which showed strong early induction in STS-treated XX plants
469 (IMFs; $\log_2$FC = 6.03 at Day 1) and remained significantly upregulated at Day 14 ($\log_2$FC = 1.90),
470 suggesting a role in both initiating and stabilizing masculinization (Table 2 & Figure 5).
471 Normalized data showed a sharp spike in *CsACS1* transcript abundance at Day 1 in IMFs (Figure
472 4C), accompanied by a modest increase in ACC concentration (Supplemental Figure 4), supporting
473 its role as a plasticity-associated ethylene biosynthesis gene. *CsACS1* remained minimally
474 expressed across all other tissues and treatments, including MFs and IFFs.

475

476 Comparative studies in other ethylene-sensitive species provide context for these dynamics.
477 Studies in cucumber and melon have shown that disruption of specific *ACS* and *ACO* genes can
478 alter floral sex ratios and reduce ethylene production, highlighting their context-dependent roles
479 in sex expression. In cannabis, *CsACS1* and *CsACO5* may act as stabilizers, with *CsACS1* showing
480 early and persistent upregulation, and *CsACO5* induced specifically at Day 14, together promoting
481 male floral development or suppressing female identity. Floral ethylene dynamics are also linked
482 to developmental timing, with genes delaying senescence indirectly modulating ethylene output.
483 For example, predicted orthologs of Arabidopsis *FOREVER YOUNG FLOWER* (*FYF*), *CsFYF2*
484 (LOC115706939) and *CsFYF4* (LOC115717309), were consistently upregulated in
485 phenotypically female flowers (FFs and IFFs). FYF transcription factors are known to repress
486 ethylene-mediated senescence and abscission pathways, extending floral longevity in early
487 developmental stages (Chen et al. 2021). Similarly, Shi *et al*. (2024a) reported elevated *CsFYF2*
488 —LOC115706939, annotated as *CsSOC1*—in female meristems and flowers, complementing our

489 observation of significantly lower *CsFYF2/4* expression in MFs and IMFs (Table 2). These
490 expression trends align with the longevity role of *FYF* proposed in other species, and the shorter
491 developmental lifespan of male cannabis inflorescences compared to female ones (Shi et al.,
492 2024a). These findings support a model in which *CsACO5* and *CsACS1* stabilize male floral
493 identity during inflorescence development, while *CsFYF2* and *CsFYF4* modulate sex-specific
494 senescence trajectories in a phenotype-dependent manner.

495

496 Upstream of both *ACS* and *ACO* activity, the Yang cycle contributes essential precursors for
497 ethylene biosynthesis. One gene in this pathway, *CsMAT2*, an autosomal Yang cycle gene located
498 on chromosome 2, encodes methionine adenosyltransferase (MAT or SAMS), which synthesizes
499 S-adenosylmethionine (SAM)—the first substrate used by ACS in ethylene biosynthesis (Figure
500 2A). *CsMAT2* was significantly downregulated in IMFs compared to FFs at Day 14 ($\log_2$FC = –
501 2.48), a developmental window coinciding with early pollen maturation (DiMatteo et al. 2020 &
502 Figure 1), suggesting a potential role in male gametophyte development. This is supported by
503 findings in Arabidopsis and rice, where *MAT* gene disruption impairs pollen tube growth, male
504 fertility, and seed set (Chen et al. 2013, 2016b). This is especially relevant in *C. sativa*, where STS-
505 induced male flowers often exhibit poor pollen quality (Lubell and Brand 2018; DiMatteo et al.
506 2020). Notably, in pumpkin, a long non-coding RNA has been shown to stabilize SAMS protein
507 and promote fruit development via ethylene biosynthesis (Tian et al. 2024), illustrating how *MAT*
508 regulation can directly modulate ethylene-dependent outcomes.

509

510 Beyond its potential functional relevance, *CsMAT2* also shows interesting network and
511 evolutionary characteristics. *CsMAT2* had strong connectivity in the XX network (kME = 0.81)
512 but weaker integration in XY plants (kME = 0.48). It also had the highest nucleotide diversity
513 among ERGs ($\pi = 5.99 \times 10^{-3}$), exceeding the genome-wide average (Supplementary Table 12).
514 This may reflect relaxed selection on *CsMAT2* due to redundancy in the *MAT* gene family as four
515 *MAT/SAMS* genes are present in the *C. sativa* genome (Figure 2B). A similar pattern occurs in
516 tomato, where distinct *SlMAT* paralogs exhibit tissue- and stage-specific expression during
517 ethylene-mediated fruit ripening (van de Poel et al. 2012). These findings suggest that *CsMAT2*

518 may represent a functionally specialized member of the *MAT* family in cannabis, with a potential
519 role in early floral development that merits further investigation.

520

521 Genomic context of plasticity: ERG distribution and chromosomal 522 constraints

523 The spatial distribution of ERGs across the genome provides insights into the genetic architecture
524 underlying sexual plasticity. Of the 47 ERGs identified, 12 were sex-linked: six in the
525 pseudoautosomal region (PAR) and six within the non-recombining SDR of the X chromosome
526 (Figure 2A), with none in the Y-linked SDR. Although suppressed recombination typically reduces
527 nucleotide diversity in SDR regions relative to the PAR, we observed unexpectedly lower
528 nucleotide diversity among PAR-located ERGs ($\theta\pi = 1.46 \times 10^{-3}$) compared to SDR ERGs ($\theta\pi =$
529 1.77×10^{-3}). Both regions exhibited nucleotide diversity levels below the autosomal ERG average
530 ($\theta\pi = 3.23 \times 10^{-3}$), suggesting strong purifying selection on PAR-localized genes, particularly
531 *CsMTK1*, *CsRTE1*, and *CsMTN/MTN-LIKE1*, which lack autosomal homologs in their respective
532 enzymatic pathways. These genomic patterns highlight how chromosomal localization shape ERG
533 function during sexual plasticity.

534

535 **ERGs in the sex-determining region (SDR)**

536 All six X-specific ERGs within the SDR have homologs elsewhere in the genome (Figure 2A),
537 functioning either in ethylene biosynthesis (*CsACS3-LIKE* and *CsACO5*) or signaling (*CsETR1*,
538 *CsCTR1*, *CsEBF1*, and *CsEIL1*). *CsACO5*, previously discussed as a key stabilizer of male floral
539 identity in XX plants, and *CsEBF1* are particularly noteworthy for their localization to the SDR.
540 This genomic configuration is reminiscent of sex-determining regions in other dioecious species,
541 such as kiwifruit (*Actinidia*), where lineage-specific duplication events gave rise to genes acquiring
542 novel, sex-specific functions through regulatory divergence (Akagi et al. 2018). In cannabis,
543 *CsACO5* and *CsEBF1*, emerged as candidate regulators of sexual plasticity (Table 2). *CsEBF1* and
544 its autosomal counterpart, *CsEBF2*, encode F-box proteins that target the *EIN3/EIN3-LIKE* (*EIL1-*
545 *3*) transcription factor family for degradation, acting as negative regulators of ethylene signaling
546 in its absence (Binder 2020). Unlike the canonical Arabidopsis model where EBF mRNA is

547 suppressed upon ethylene exposure (An et al. 2010), both cannabis homologs were unexpectedly
548 upregulated in ethephon-treated IFFs at Day 1 (*EBF1* $\log_2$FC = 1.71; *EBF2* $\log_2$FC = 1.33). By
549 Day 14, *CsEBF1* was also significantly upregulated in IMFs, a pattern not shared by *CsEBF2*.
550 *CsEBF1* expression in sex changed flowers (day 14) suggests a potential role in stabilizing
551 masculinization by suppressing ethylene signaling. As an SDR-linked gene, its regulation may be
552 influenced by sex chromosome context, but further research is needed to determine whether this
553 reflects sex-specific control or a more general role in floral development under STS treatment.

554

555 **ERGs in the pseudoautosomal region (PAR)**

556 We identified six ERGs shared within the PAR of the X and Y chromosomes. Among them, *MTN,*
557 which is essential for recycling methylthioadenosine (MTA), a byproduct of the first committed
558 step in ethylene biosynthesis. *CsMTN* and *CsMTN-LIKE1* were located within a WGCNA module
559 correlated with sexual plasticity treatment in XX plants (r = 0.66) and with high module
560 membership (kME = 0.73 and 0.79, respectively), supporting their centrality in the transcriptional
561 response to masculinization. Both genes were significantly upregulated in IMFs relative to
562 untreated XX controls ($\log_2$FC = 1.14 and 1.17), while IFFs showed significant downregulation
563 relative to XY controls ($\log_2$FC = -1.01 and -1.10; Table 2). These findings align with our previous
564 study showing floral organ concordant expression of *MTN* (Monthony et al. 2024) and with Borin
565 *et al*. (2024), who reported high *CsMTN* expression in MF and IMFs. In Arabidopsis, functional
566 analyses have shown that *MTN* is required for male fertility: double mutants of *mtn1-1 mtn2-1*
567 exhibit indehiscent anthers and malformed pollen grains (Waduwara-Jayabahu et al. 2012). In
568 dioecious *Amborella trichopoda*, transcriptomic analyses of immature flowers revealed
569 differential expression of *AmbMTN* by sex, with higher expression in female tissues (Carey et al.
570 2024a). Whether this response reflects direct ethylene regulation or secondary developmental
571 reprogramming remains to be clarified, as Yang cycle gene responsiveness to ethylene varies
572 across species (Bürstenbinder et al. 2007; van de Poel et al. 2012)

573

574 To further assess the role of methionine recycling during sexual plasticity, we next examined
575 *CsMTK1*, a downstream Yang cycle enzyme also localized in the PAR (Figure 2A). *CsMTK1*

576 phosphorylates 5-methylthioribose (MTR), a product of MTN activity, to form 5-
577 methylthioribose-1-phosphate (Figure 2B). Only one *MTK* is present in *C. sativa*, consistent with
578 *A. thaliana*, *Plantago major* L., and several other species (Pommerrenig et al. 2011; Chen et al.
579 2025a). Whereas *CsMTN* and *CsMTN-LIKE1* were strongly connected to plasticity modules in
580 both XX and XY networks, *CsMTK1* expression was XX-specific (*kME* = –0.74) and weakly
581 connected in XY plants (*kME* = 0.28), suggesting limited involvement in male-to-female
582 transitions. *CsMTK1* was significantly downregulated in IMFs compared with FFs ($\log_2$FC = –
583 1.47), with no significant change between IFFs and MFs. This Day 14-specific downregulation
584 suggests *CsMTK1* is developmentally, rather than ethylene, regulated. This aligns with
585 Arabidopsis and rice, where MTK is essential for SAM recycling under sulfur limitation but not
586 induced by ethylene (Bürstenbinder et al. 2007; Rzewuski et al. 2007). By contrast, *MTK*
587 expression is ethylene-responsive in climacteric species such as tomato and cucumber, pointing to
588 a species-specific regulatory architecture (van de Poel et al. 2012; Chen et al. 2025a). In *Cannabis*,
589 these patterns support a functional decoupling between *CsMTN* and *CsMTK1* during sexual
590 plasticity, wherein MTA cleavage via MTN is prioritized while methionine recycling through
591 MTK1 is developmentally downregulated. Supporting this, *CsMTK1* exhibited elevated nucleotide
592 diversity ($\pi = 4.58 \times 10^{-3}$), higher than both the PAR ERG average and genome-wide mean
593 (Supplementary Table 12), suggesting relaxed purifying selection relative to *CsMTN*. Together,
594 the gene expression and diversity data suggest *CsMTK1* may be dispensable for ethylene-mediated
595 sex change in *Cannabis*.

596

597 The final candidate ERG located in the PAR is *CsRTE1*, a known negative regulator of ethylene
598 signaling. Unlike the Yang cycle genes discussed above, which may play a role in modulating the
599 biosynthetic capacity of the pathway, *CsRTE1* acts in the ethylene signaling pathway, appearing
600 as a responsive gene rather than a driver of sexual plasticity. In our study, *CsRTE1* was
601 significantly upregulated in XY leaf tissue one day after ethephon treatment (Day 1 IFFs), a pattern
602 not observed in treated XX plants. This response is consistent with previous findings in
603 *Arabidopsis*, where *RTE1* is induced by ethylene and functions in a feedback loop to stabilize the
604 *ETR1* receptor and attenuate downstream signaling (Resnick et al. 2006). The transient
605 upregulation of *CsRTE1* in XY plants may reflect a mechanism for buffering early ethylene

signaling—in this case in response to ethephon treatment—and preventing an overactivation of the autocatalytic ethylene biosynthesis loop. Supporting this, ACC concentrations in Day 1 IFFs were not significantly elevated compared to untreated XY plants (Supplemental Figure 4), suggesting that ethephon application does not trigger a runaway ethylene biosynthesis response within first 24 hours following ethephon treatment. Instead, *CsRTE1* may help temper responses to exogenous ethephon applications, maintaining signaling homeostasis as phenotypic feminization is initiated.

Convergent phenotypes, divergent mechanisms: A phase-dependent model

The integration of temporal transcriptomic patterns, pathway-specific metabolite data (ACC), and ERG genomic localization underscores the modularity and adaptability of the ethylene response network in *Cannabis*. Despite a shared hormonal signaling pathway, XX and XY *Cannabis sativa* plants follow distinct molecular trajectories during sex change yet converge on similar phenotypic outcomes: the production of opposite-sex flowers. This apparent contradiction of convergent floral phenotypes arising from divergent gene expression programs, is a central finding of this study, and supports a refined, phase-dependent model of ethylene-regulated sexual plasticity in *C. sativa* (Figure 5).

In this model, plasticity begins prior to floral primordia emergence, shortly after STS or ethephon application and photoperiod shift. This initiation phase is marked by broad but sex-specific upregulation of ethylene biosynthesis and signaling genes. Shared early responders include *CsACO3* (upregulated in both XX and XY contexts), *CsACS1* and *CsERF1* in IMFs, and *CsACS2*, *CsRTE1*, and both *CsEBF1/2* in IFFs. These genes likely initiate developmental reprogramming by shifting the hormonal balance toward a new sex-specific pathway.

In the subsequent stabilization phase, distinct ERGs help maintain the new phenotypic identity. In masculinized XX plants, *CsACO5*, *CsMTN*, and *CsACS1* remain upregulated, supporting male

634 floral development. In feminized XY plants, upregulation of *CsFYF2* and *CsFYF4* may suppress
635 senescence and promote female organ longevity. These stabilization-phase genes often show sex-
636 biased expression, with some (e.g., *CsACO5*, *CsEBF1*) located in the SDR and others (e.g.,
637 *CsMAT2*, *CsERF1*) on autosomes. These findings suggest that ethylene-mediated plasticity is not
638 governed by a single sex-linked switch, but rather arises from distributed, tissue- and time-specific
639 regulatory modules.

640

641 Our multi-omic analysis provides the first temporally resolved, genome-informed framework for
642 ethylene-mediated sex change in *Cannabis sativa*. By capturing both conserved and sex-specific
643 ERG responses across genotypes, we identify key plasticity initiators (e.g., *CsACO3*, *CsERF1*),
644 stabilizers (e.g., *CsACO5*, *CsACS2, CsFYF2/4*), and dual-phase regulators (*CsACS1*), and propose
645 a working model for understanding ERG function in sexual plasticity (Figure 5). The study also
646 highlights candidate sex-specific regulators such as *CsMAT2*, *CsMTN*, and *CsMTK1* in XX
647 contexts, and *CsRTE1* and *CsEBF2* in XY plants. Looking ahead, spatial transcriptomics and
648 functional validation through gene silencing or editing will be critical to dissect causal roles within
649 this regulatory network and advance the development of sex-stable genotypes for breeding and
650 cultivation. As our understanding deepens, future models should also incorporate the likely
651 crosstalk between ethylene and other plant growth regulators, such as gibberellins and cytokinins,
652 which are known to influence sex expression in *Cannabis sativa*.

653

654 Materials & Methods

655 Plant selection and vegetative growing conditions

656 Vegetative mother and father plants from three commercially available drug-type genotypes—*La*
657 *Rosca*, *Panama Pupil V4*, and *Deadly Kernel*—were greenhouse-grown, cloned, and rooted for
658 two weeks under LED lighting (Phlizon, China) in moistened stone wool (Indoor Farmer, Canada)
659 beneath vented plastic humidity domes. Rooted clones were then transferred to 10 cm square pots
660 filled with sterilized Pro-Mix BX (Pro-Mix, Canada) and maintained under controlled environment

661 conditions in growth chambers (Conviron, Canada) for 10 days to allow root establishment. During
662 this period, plants were watered by hand as needed.

663 Subsequently, plants were transplanted into 4-litre round pots and grown for 12 days under a 12/12
664 day/night photoperiod with drip irrigation adjusted weekly. Thereafter, the photoperiod was shifted
665 to 18/12 to induce flowering. Photosynthetic photon flux density (PPFD), as well as day and night
666 humidity levels, were gradually decreased throughout the experiment, reaching a maximum of 750
667 µmol/m²/s at canopy height, as detailed in Supplementary Table 1. The pH of the growth substrate
668 was monitored weekly and maintained between 5.5 and 6.0, adjusted as necessary using 1.5 g/L
669 of elemental sulfur during watering. A complete description of growing conditions, including
670 photoperiod, light intensity, and fertigation regimes, is provided in Supplementary Table 1.

671

672 Plant sexing

673 Samples were taken from 6-month-old vegetative mother and father plants, in all three drug-type
674 genotypes to confirm the chromosomal sex. Approximately 50 mg of young leaf tissue was
675 harvested for DNA extraction and desiccated for four days using Drierite (Xenia, OH, USA). The
676 dried tissue was ground using metallic beads in a RETSCH MM 400 mixer mill (Fisher Scientific,
677 MA, USA) and DNA was extracted using a CTAB-chloroform protocol (Lapierre et al. 2023b).
678 Briefly, powdered tissue was treated with CTAB buffer, followed by phenol-chloroform
679 extraction. The resulting DNA pellet was washed with ethanol, resuspended in water, and
680 quantified using a Qubit fluorometer with the dsDNA HS assay kit (Thermo Fisher Scientific,
681 Waltham, MA, USA). DNA concentrations were adjusted to 10 ng/µL.

682

683 Sex determination was performed using PCR Allelic Competitive Extension (PACE, 3CR
684 Bioscience Ltd) assay using CSP-2 primers (Supplementary Table 2) and methodology as
685 described in Toth (2022), and Toth *et al.* (2020). PACE reactions were performed with PACE 2.0
686 Genotyping Master Mix (3CR Bioscience Ltd) and thermally cycled according to the
687 manufacturer's instructions, with five extra final cycles (i.e. a total of 35 cycles of denaturation,
688 annealing and extension) on the Applied Biosystems Veriti Thermal Cycler. Post-PCR

689 fluorescence signals were detected with the Applied Biosystems 7500 Real-Time PCR System and
690 analyzed using Applied Biosystems 7500 Software v2.3.

691

692 Plant flowering and sex plasticity induction

693 All plants were cultivated under LED lighting in controlled-environment growth chambers. To
694 prevent pollination and accommodate space constraints, plants were grown in two separate batches
695 under identical conditions (Supplementary Table 1). The first batch contained male flowering
696 treatments: MF (XY) and IMF (XX), while the second batch contained female flowering
697 treatments: FF (XX) and IFF (XY). Induction of sexual plasticity in XX plants was performed
698 using STS, following the protocol of Jones & Monthony (2022). A 3 mM silver thiosulfate (STS)
699 solution with 0.1% Tween 20 was prepared from sodium thiosulfate (Fisher Chemical, Fair Lawn,
700 NJ, USA) and silver nitrate (Fisher Chemical, USA). The solution was applied as a foliar spray
701 (~50 mL per plant) once per week for three weeks, ensuring thorough leaf coverage. The first
702 application coincided with the photoperiod shift, immediately after the first 12-hour night, and all
703 subsequent treatments were administered immediately after growth chamber lights extinguished
704 in order to prevent leaf burning.

705

706 Induction of sexual plasticity in XY plants was achieved using 500 mg/L ethephon, adapted from
707 Moon et al. (2020). The treatment solution was prepared from a 40% aqueous solution of ethephon
708 (2-chloroethylphosphonic acid; AK Scientific, Union City, CA, USA), by diluting it in distilled
709 water to the final concentration (500 mg/L; 8.65 mM) with 0.1% Tween 20 as a surfactant. Plants
710 were sprayed to saturation (~50 mL per plant) in a single application, administered immediately
711 after the photoperiod shift when growth chamber lights extinguished, to prevent leaf burning. In
712 both batches, control plants (MF and FF) were sprayed to saturation with distilled water containing
713 0.1% Tween 20 to ensure comparable treatment conditions.

714

715 # Floral development and quantification of sexual plasticity

716 Floral development was tracked weekly for 28 days following floral induction. Representative
717 floral clusters were selected from the top half of the plant for macroscopy. Plants were visualized
718 using an Olympus SZX16 macroscope (Olympus Corp., Japan) and photographed with an
719 Olympus DP21 camera. Sexual plasticity was quantified by determining the ratio of flowers on six
720 randomly selected inflorescence segments measuring 3 cm whose phenotypic sex no longer
721 matched the plants genotypic sex. This was done following 28 days of flowering. For control plants
722 (MF and FF), which displayed no sexual plasticity, one randomly selected inflorescence segment
723 was selected.

724

725 Floral sex ratios were calculated in R (v4.1.1). A two-way fixed effects analysis of variance
726 (ANOVA) was conducted. Sex change (%) was the response variable, genotype and phenotypic
727 floral sex were the independent variables. Prior to analysis of variance, the sex change data were
728 transformed using an arcsine square root transformation (McDonald 2014), as the datasets for sex
729 change (in percentiles) were highly clustered at 0 and 1, and the arcsine square root model shows
730 less dramatic variance at the end of the distribution (Monthony et al. 2021a). Means comparisons
731 was performed using a Tukey-Kramer post-hoc test (Kramer 1956) to account for multiple
732 comparisons. Post-hoc means comparisons were visualized using the *multcompLetters4* from the
733 multcompView package (Piepho 2004). Bar plots of the average sex change were generated with
734 ggplot2 (v3.4.1; Wickham 2009) using the Paired colour palette from RColorBrewer (Brewer et
735 al. 2002).

736

737 # Cannabinoid quantification

738 Cannabinoid quantification was performed using an established UPLC-PDA method, as
739 previously described by Lapierre et al. (2023b), at the Metabolomics Platform, Institute of
740 Nutrition and Functional Foods (INAF), Université Laval, Québec, QC, Canada. In brief, plants
741 were grown under standard greenhouse conditions to maturity, as outlined in Lapierre et al.
742 (2023b) and mature female (XX) flowers (~5 g) were collected, trimmed and dried for analysis. A
743 subsample (200 mg) was extracted in 25 mL of 80% methanol (Thermo Fisher Scientific,

744 Optima™ HPLC ≥99%) by sonication for 15 min. Extracts were centrifuged at 4500 × g for 5 min,
745 and the supernatant was filtered through a 0.22 µm nylon filter before being diluted by factors of
746 2 and 20.

747

748 Cannabinoid analysis was performed using a Waters Acquity I-Class UPLC system with a
749 photodiode array (PDA) UV detector. Separation was achieved on a Cortecs 1.6 µm, 2.1 mm ×
750 150 mm column (Waters Corporation, Milford, MA, USA) with a Cortecs C18 pre-column
751 (Waters Corporation, 90Å, 1.6 µm, 2.1 mm X 5 mm) maintained at 30°C. The mobile phase
752 consisted of (A) 20 mM ammonium formate (Thermo Fisher Scientific, Optima LC/MS ≥99%),
753 acidified to pH 2.92 with formic acid (MS grade) and diluted with Mili-Q water (Thermo Fisher
754 Scientific) and (B) 100% acetonitrile (Milipore Sigma, OmniSolv® LC/MS ≥99.9%), with a
755 gradient elution program as follows: 0–6.4 min, 76% B; 6.5–8 min, 99% B; 8.1–10 min, re-
756 equilibration at 76% B. The flow rate was set at 0.45 mL/min, and the injection volume was 1 µL.
757 Detection was performed at 228 nm, and quantification was based on 5-point calibration curves
758 (1–100 mg/L) for all cannabinoid standards.

759

760 Standard calibration curves were prepared by diluting a mix of cannabinoid standards in 80%
761 methanol. A 500 µL stock solution at 100 mg/L was prepared by combining 50 µL of each
762 individual standard from stock solutions at 1000 mg/L and adjusting the final volume with 80%
763 methanol. Serial dilutions were then performed to generate calibration points at 100, 50, 25, 5, and
764 1 mg/L. Details of the cannabinoid standards are provided in Supplementary Table 3.

765

766 Quantification of ACC and SAM

767 A detailed methodological description of standards preparation, derivatization, and
768 chromatographic conditions is provided in the Supplementary Materials and the accompanying
769 parameters can be found in Supplementary Table 4 through Supplementary Table 7. SAM and
770 ACC concentrations were quantified against standard calibration curves prepared from serial
771 dilutions of frozen stock standards, and lysine was included as an internal derivatization control

772 (Supplementary Table 4). Leaf tissues (n = 3 biological replicates per genotype, treatment, and
773 time point) were harvested on day 0 and day 1, flash frozen, and extracted using a trichloroacetic
774 acid (TCA) protocol (Bishop et al., 2024; Sandhu et al., 2024). Approximately 50 mg of leaf tissue
775 was homogenized in 1 mL TCA, centrifuged, and filtered. Supernatants were derivatized using 6-
776 aminoquinolyl-N-hydroxysuccinimidyl carbamate (AQC; Supplementary Table 4) and analyzed
777 via UPLC-MS/MS on a Waters Acquity I-Class UPLC and Xevo TQ-S system (Supplementary
778 Table 5 & Supplementary Table 6). Chromatographic separation was performed on a BEH C18
779 column, and analytes were detected in positive ESI mode using multiple reaction monitoring
780 (MRM; Supplementary Table 7). SAM and ACC data processing for quantification was performed
781 using TargetLynx V4.1.

782

783 Statistical analysis of ACC and SAM data

784 Variance stabilizing transformation (VST) of gene expression data was correlated with measured
785 ACC levels using Spearman's rank correlation within each treatment group. Genes with zero
786 variance were excluded, and outliers (Studentized residuals > ±3.4) were removed. FDR correction
787 was applied to p-values, and only genes with $|\rho| \geq 0.5$ and FDR-adjusted $p \leq 0.05$ in at least one
788 group were visualized. ACC concentrations were also analyzed using a linear mixed-effects model
789 including treatment, sex, and day as fixed effects, and sample ID nested within genotype as a
790 random effect. Tukey's HSD post-hoc test was applied to estimated marginal means. SAM was
791 below the limit of quantification in all samples and was not included in downstream analyses. Full
792 statistical methods, R package versions, and model diagnostics are available in the Supplementary
793 Materials.

794

795 ERG Identification

796 Identification of ERG in *C. sativa* was previously conducted using an *in silico* ortholog analysis
797 by Monthony *et al.* (2024), based on the *C. sativa* cs10 reference genome (RefSeq assembly
798 accession: GCF_900626175.2; Grassa et al. 2021). We improve upon this dataset by applying the
799 same methodology to newly available genomic resources, including the *C. sativa* 'Pink Pepper'
800 XX reference genome (NCBI 2023) and the haploid X and Y whole genomes for the genotype

801 ‘Otto II’ (Carey et al. 2024b). Briefly, ERG orthologs were identified using OrthoFinder (Emms
802 and Kelly 2015) and BLASTP (Altschul et al. 1990), as described in Monthony et al. (2024),
803 followed by manual curation. Chromosome maps were generated with the chromoMap (v4.1.1;
804 Anand and Rodriguez Lopez 2022) package in R.

805

806 Whole genome sequencing and variant calling

807 Fresh leaf tissues obtained from one male (XY) and one female (XY) individual of the three
808 genotypes were used for DNA extraction using the Qiagen DNeasy Plant Mini kit (Qiagen GmbH,
809 Germany). For whole genome sequencing (WGS), six libraries were prepared at the Institut de
810 biologie intégrative et des systèmes (IBIS), Université Laval, QC, Canada. The sequencing was
811 conducted on an Illumina NovaSeq 6000 (Illumina, CA, USA) with 150 bp paired-end reads at the
812 Genome Quebec Service and Expertise Center (CESGQ), Montreal, QC, Canada, with an average
813 coverage of approximately 30x per sample.

814

815 Reads were mapped on the *C. sativa* ‘Pink Pepper’ reference genome (NCBI 2023) with *bwa mem*
816 version 7.17 (Li 2013). Variant calling was performed with Fast-WGS (Torkamaneh et al. 2018)
817 and manta version 1.6 (Chen et al. 2016a) for nucleotide and structural variant calling, respectively.
818 Raw variant data were filtered with VCFtools version 1.16 (Danecek et al. 2011) to remove low-
819 quality variants (filter PASS, QUAL <10, MQ <30, MinDP <6, MAF 1%). Variants within ±5 kb
820 of CsERGs in the *C. sativa* ‘Pink Pepper’ reference genome (NCBI 2023) were filtered using
821 BEDtools v2.31.1 (Quinlan and Hall 2010). Functional impact of variants in ±5 kb around of
822 CsERGs were investigated using the Ensembl Variant Effect Predictor (McLaren et al. 2016) with
823 the GFF of Pink Pepper (NCBI 2023). Consequence terms (e.g., inframe insertion, missense
824 variant, synonymous variant) and the impact rating are based on Sequence Ontology (Eilbeck et
825 al. 2005). Impact ratings are classified as (i) Modifier correspond to variant affecting non-coding
826 sequences, (ii) Low correspond to variant unlikely to change protein behaviour, (iii) Moderate
827 correspond non-disruptive variant that might change protein effectiveness, and (iv) High
828 correspond to variants probably causing protein truncation and/or loss of function. The nucleotide
829 diversity (π; Nei & Li, 1979) in a sliding windows of 1000 bp and Tajima’s D value in bins with

830 size of 10,000 SNPs were estimated using VCFtools (Danecek et al. 2011). Gene with less than 2
831 SNPs were excluded from the diversity analysis.

832

833 RNA extraction & sequencing

834 Leaf tissues were consistently sampled from mature leaves, in the middle section of the plant.
835 Representative floral tissues (day 14) were consistently sampled from upper most axillary branch
836 of the plants. Immediately after harvesting, plant tissues were flash-frozen in liquid nitrogen and
837 hand-ground using a disposable cryosafe pestle in 2 mL RNase-free tubes to preserve RNA
838 integrity. Total RNA was extracted using the RNeasy Plant Mini Kit (Qiagen), following the
839 manufacturer's protocol with modifications to enhance RNA purity. Briefly, 25–50 mg of ground,
840 frozen tissue was combined with RLC buffer and β-mercaptoethanol, as per the manufacturer's
841 recommendations, and vortexed until homogenized. To improve purity, an additional wash with
842 buffer RPE (Qiagen) was included in the final wash step. RNA was quantified
843 spectrophotometrically using a NanoDrop spectrophotometer (Thermo Fisher Scientific). RNA
844 quality was assessed visually, via electropherograms from the 2100 Bioanalyzer (Agilent
845 Technologies, Santa Clara, CA, USA), and quantitatively, using the RNA Integrity Number (RIN;
846 Supplementary Table 8). High-quality RNA samples were converted to cDNA using the
847 NEBNext® Ultra™ II Directional RNA Library Prep Kit for Illumina (New England Biolabs,
848 Ipswich, MA, USA). Library preparation and sequencing were conducted at the Institut de
849 Biologie Intégrative et des Systèmes (IBIS), Université Laval, Quebec, Canada. Sequencing was
850 performed on an Element Biosciences AVITI platform (Element Biosciences, San Diego, CA,
851 USA), generating 150 bp paired-end reads, with an average output of ~30 million reads per sample.
852 In total, 138 samples passed quality control and were used in all future analyses (Supplementary
853 Table 8).

854

855 Transcriptomic analysis

856 RNA sequencing quality was assessed using FASTQC (v0.11.8), and trimming of low-quality
857 bases was performed in paired-end mode using Trimmomatic (v0.39) with the following
858 parameters: adapter trimming (ILLUMINACLIP), a mismatch seed value of 2, a palindrome clip

859 threshold of 30, a simple clip threshold of 10, and a minimum read length (MINLEN) of 40. For
860 rare RNA samples identified with foreign RNA contamination based on overrepresented sequences
861 and skewed GC ratios, contaminant sequences were extracted for further analysis. These sequences
862 were classified by species using a BLAST search against the NCBI nucleotide database, with
863 duplicates filtered and mapped to unique organisms. Non-plant contaminants, such as animal and
864 fungal sequences, were removed using a modified Trimmomatic script with a custom contaminant
865 sequence list. The trimming process retained ~95% of paired reads, and post-trimming quality was
866 re-assessed using FastQC to confirm improvements in sequence composition.

867

868 Alignment of paired-end reads was performed as described in Monthony et al. (2024) with
869 modifications. Briefly, reads were aligned to the *C. sativa* "Pink Pepper" v1 genome (NCBI) using
870 STAR (v2.7.11b) and output as coordinate-sorted BAMs (--outSAMtype BAM
871 SortedByCoordinate). Immediately after each sample finished mapping, they were aligned with
872 Samtools (v1.15) to retain only alignments with MAPQ ≥ 30 (samtools view -b -q 30), yielding
873 high-confidence BAMs for downstream counting. Gene-level counts were then obtained with
874 HTSeq-count (v2.0.2; Putri et al. 2022) in positional mode (-r pos), using a stranded setting (-s
875 yes), a minimum alignment quality filter of 30 (-a 30), and exon features (-t exon) keyed by gene
876 IDs (-i gene).

877

878 **Principal component analysis and gene expression visualization**

879 Principal component analysis (PCA) was performed on the VST normalized, batch-corrected
880 counts of 47 selected genes of interest, obtained from gene-level counts following alignment and
881 quantification. VST transformation was applied using the DESeq2 package (v1.42.1; Love et al.
882 2014) to normalize the gene expression data. The first two principal components (PC1 and PC2)
883 were extracted and plotted to visualize the clustering of samples based on their gene expression
884 profiles. PCA plots were generated using the ggplot2 package (v3.5.1), with ellipses representing
885 95% confidence intervals for each treatment group.

886

887 For heatmap preparation, the filtered gene expression data was scaled by row (z-score
888 transformation) using the pheatmap package (v1.0.12) to normalize gene expression levels across
889 samples. Hierarchical clustering of genes and samples was performed using Euclidean distance
890 and complete linkage to reveal patterns in gene expression across different treatments and time
891 points.

892

893 **Network analysis (WGCNA)**

894 Weighted Gene Co-expression Network Analysis (WGCNA) was performed to construct sex-
895 specific gene co-expression networks, identifying gene expression patterns associated with sex-
896 change treatments. All analyses were performed in R (v4.3.3) using the WGCNA package (v1.73;
897 Langfelder and Horvath 2008). Networks were built separately for male (XY) and female (XX)
898 samples, using count data processed through multiple quality control and normalization steps to
899 ensure data integrity.

900

901 Prior to network construction, outlier genes and samples were detected and removed using the
902 goodSamplesGenes (gsg) function in WGCNA, which identifies genes and samples with excessive
903 missing values or abnormal expression patterns (see Supplementary Table 8). To further validate
904 sample quality, hierarchical clustering and principal component analysis (PCA) were used to
905 identify additional outlier samples, which were subsequently removed. Following outlier removal,
906 batch correction was performed using a DESeq2-based method (Roy et al. 2025). Additionally,
907 low-count genes were filtered using HTSFilter (v1.42.0; Rau et al. 2013), which dynamically
908 adjusts filtering thresholds based on dataset structure rather than applying an arbitrary cutoff. After
909 filtering, the data were normalized using variance stabilizing transformation (VST) to reduce
910 heteroscedasticity and improve network construction.

911

912 To determine an appropriate soft-thresholding power, the pickSoftThreshold function was applied
913 independently to each subset to ensure scale-free topology (signed $R^2 > 0.80$ with minimal mean
914 connectivity). Based on topology evaluation, a soft-thresholding power of 6 was selected for XX
915 and 7 for XY datasets. Networks were constructed using blockwiseModules, employing a signed

916 adjacency matrix, a module merging cut height of 0.20, with a maximum block size of 30,000 and
917 modules were identified using dynamic tree cutting.

918

919 Module-trait correlation, adapted from Wang *et al.* (2020), was performed independently for XX
920 and XY networks to identify biologically relevant gene clusters associated with sex-altering
921 treatment. Treatment was defined as STS application in the XX network and ethephon application
922 in the XY network. To prioritize biologically relevant gene modules, modules significantly
923 correlated with treatment ($|r| \geq 0.5$, $p \leq 0.05$) were retained for further analysis (Wang et al. 2020).
924 To assess whether treatment-associated modules exhibited temporal specificity, their correlation
925 with time points was examined. Time points were analyzed using a "Day vs. all" approach, where
926 Day 1 and Day 14 were each compared to all other time points. Day was treated as a categorical
927 variable with Day 0 as the baseline, while treatment was encoded as a binary variable (1 = treated,
928 0 = control). A shortlist of ethylene-related genes (ERGs) was generated by extracting those
929 present in highly correlated modules. For each ERG, intra-modular connectivity (kME) was
930 calculated to assess its centrality within its respective module. The final list of ERGs from highly
931 correlated modules in both XX and XY networks was retained for subsequent differential gene
932 expression analysis.

933

934 **Differential gene expression analysis**

935 Differential gene expression (DGE) analysis was performed using DESeq2 to identify genes
936 exhibiting significant expression changes in response to ethephon and STS treatments across male
937 (XY) and female (XX) plants, respectively. DGE was focused on candidate ERGs identified in
938 WGCNA. Raw count data were preprocessed by filtering low-expression genes using HTSFilter
939 (Rau et al. 2013). Normalized counts were obtained using a VST. Batch effects were modeled as
940 a fixed effect in the DESeq2 generalized linear model (GLM) to correct for potential variation
941 across experimental batches. Pairwise contrasts were constructed to evaluate: (1) STS-treated IMF
942 (XX) vs. untreated FF (XX), (2) ethephon-treated IFF (XY) vs. untreated MF (XY), and (3)
943 baseline differences between control MF (XY) and FF (XX) samples. Custom contrast vectors
944 were applied to account for sex, treatment, and batch effects, ensuring robust comparisons. The

$\log_2$ fold-change ($\log_2$FC) for each contrast was shrunk using ashr (Stephens 2017) to provide more stable effect size estimates, particularly for low-expression genes.

Genes were considered significantly differentially expressed if they met the criteria of adjusted p-value (padj) ≤ 0.05 and absolute $\log_2$FC ≥ 1 (Monthony et al. 2024; Shi et al. 2024b). Differentially expressed genes were further filtered to only include those differentially expressed across all three genotypes, ensuring treatment effects were not genotype dependent. Visualization of DGE results included bar plots of $\log_2$FC values, highlighting genes with significant changes across treatment conditions and time points. Additionally, variance-stabilized expression levels were plotted using boxplots to compare expression profiles across MF, FF, IMF, and IFF groups. All analyses were conducted using R (v4.3.3), and visualizations were produced using ggplot2 (v3.5.1) for data visualization, dplyr (v1.1.4) for data manipulation, and wesanderson (v0.3.7) for color palettes.

Statements and Declarations

The authors have no competing interests to declare. The authors gratefully acknowledge the support of the Natural Sciences and Engineering Research Council (NSERC) Discover Grant number RGPIN-2022-03396. ASM has also been supported by a NSERC Canada Vanier Graduate Scholarship.

Data availability statement

All raw transcriptomic data will be made available on the NCBI sequence read archive (SRA) upon publication of this manuscript.

Acknowledgements

The authors would like to thank Christian Otis and Brian Boyle at the Université Laval Genomic Analysis Platform (PAG) for their invaluable counsel on RNA extraction and Hélène Martin for her help sexing plant materials used in this study.

Author contributions

ASM and DT planned and designed the research. ASM, MdR, OC and SJM contributed to the methodology. ASM, JR, MdR and OC performed the investigation and contributed to data curation. ASM, JR, MdR conducted formal analysis. SJM and DT acquired funding for the project. ASM and DT handled project administration. SJM and DT provided resources. SJM and DT supervised the research. ASM, MdR and JR visualized the results. ASM, MdR, OC and DT wrote the original draft of the manuscript. ASM, SJM, and DT contributed to reviewing and editing the manuscript.

References

Adal AM, Doshi K, Holbrook L, and Mahmoud SS. Comparative RNA-Seq analysis reveals genes associated with masculinization in female Cannabis sativa. Planta. 2021:**253**(1):1–17. https://doi.org/10.1007/s00425-020-03522-y

Akagi T, Henry IM, Ohtani H, Morimoto T, Beppu K, Kataoka I, and Tao R. A Y-Encoded Suppressor of Feminization Arose via Lineage-Specific Duplication of a Cytokinin Response Regulator in Kiwifruit. Plant Cell. 2018:**30**(4):780–795. https://doi.org/10.1105/tpc.17.00787

Akagi T, Segawa T, Uchida R, Tanaka H, Shirasawa K, Yamagishi N, Yaegashi H, Natsume S, Takagi H, Abe A, et al. Evolution and functioning of an X–A balance sex-determining system in hops. Nat Plants. 2025. https://doi.org/10.1038/s41477-025-02017-6

Altschul SF, Gish W, Miller W, Myers EW, and Lipman DJ. Basic local alignment search tool. J Mol Biol. 1990:**215**(3):403–410. https://doi.org/10.1016/S0022-2836(05)80360-2

An F, Zhao Q, Ji Y, Li W, Jiang Z, Yu X, Zhang C, Han Y, He W, Liu Y, et al. Ethylene-induced stabilization of ETHYLENE INSENSITIVE3 and EIN3-LIKE1 is mediated by proteasomal degradation of EIN3 binding F-box 1 and 2 that requires EIN2 in arabidopsis. Plant Cell. 2010:**22**(7):2384–2401. https://doi.org/10.1105/tpc.110.076588

Anand L and Rodriguez Lopez CM. ChromoMap: an R package for interactive visualization of multi-omics data and annotation of chromosomes. BMC Bioinformatics. 2022:**23**(1):1–9. https://doi.org/10.1186/s12859-021-04556-z

Anger N, Fogliani B, Scutt CP, and Gâteblé G. Dioecy in Amborella trichopoda: evidence for genetically based sex determination and its consequences for inferences of the breeding system in early angiosperms. Ann Bot. 2017:**119**(4):591–597. https://doi.org/10.1093/aob/mcw278

Binder BM. Ethylene signaling in plants. J Biol Chem. 2020:**295**(22):7710–7725. https://doi.org/10.1074/jbc.REV120.010854

1004 **Borin M**. Overcoming challenges in Cannabis sativa breeding research with conventional and
1005 biotechnological tools THESIS. 2024.

1006 **Boualem A, Troadec C, Camps C, Lemhemdi A, Morin H, Sari MA, Fraenkel-Zagouri R,**
1007 **Kovalski I, Dogimont C, Perl-Treves R, et al.** A cucurbit androecy gene reveals how
1008 unisexual flowers develop and dioecy emerges. Science (80-). 2015:**350**(6261):688–691.
1009 https://doi.org/10.1126/science.aac8370

1010 **Brewer C, Harrower M, Sheesley B, Woodruff A, and Heyman D**. ColorBrewer 2.0. 2002.
1011 https://colorbrewer2.org. Retrieved April 11, 2023

1012 **Bürstenbinder K, Rzewuski G, Wirtz M, Hell R, and Sauter M**. The role of methionine
1013 recycling for ethylene synthesis in Arabidopsis. Plant J. 2007:**49**(2):238–249.
1014 https://doi.org/10.1111/j.1365-313X.2006.02942.x

1015 **Carey SB, Aközbek L, Lovell JT, Jenkins J, Healey AL, Shu S, Grabowski P, Yocca A,**
1016 **Stewart A, Jones T, et al.** ZW sex chromosome structure in Amborella trichopoda. Nat
1017 Plants. 2024a:**10**(December). https://doi.org/10.1038/s41477-024-01858-x

1018 **Carey SB, Bentz PC, Lovell JT, Akozbek LM, Havill JS, Padgitt-Cobb L, Lynch RC, Allsing**
1019 **N, Osmanski A, Easterling KA, et al.** The evolution of heteromorphic sex chromosomes in
1020 plants. bioRxiv. 2024b:1–28. https://doi.org/10.1101/2024.12.09.627636

1021 **Chen H, Zhao Z, Chen J, Mertens J, Van de Poel B, Li D, and Chen K**. The Yang cycle in
1022 plants: a journey of methionine recycling with fascinating metabolites and enzymes. Plant
1023 Horm. 2025a:**1**(1):0–0. https://doi.org/10.48130/ph-0025-0007

1024 **Chen WH, Jiang ZY, Hsu HF, and Yang CH**. Silencing of FOREVER YOUNG FLOWER-Like
1025 Genes from Phalaenopsis Orchids Promotes Flower Senescence and Abscission. Plant Cell
1026 Physiol. 2021:**62**(1):111–124. https://doi.org/10.1093/pcp/pcaa145

1027 **Chen X, Schulz-Trieglaff O, Shaw R, Barnes B, Schlesinger F, Källberg M, Cox AJ,**
1028 **Kruglyak S, and Saunders CT**. Manta: rapid detection of structural variants and indels for
1029 germline and cancer sequencing applications. Bioinformatics. 2016a:**32**(8):1220–1222.
1030 https://doi.org/10.1093/BIOINFORMATICS/BTV710

1031 **Chen Y, Xu Y, Luo W, Li W, Chen N, Zhang D, and Chong K**. The F-box protein OsFBK12
1032 targets OsSAMS1 for degradation and affects pleiotropic phenotypes, including leaf
1033 senescence, in rice. Plant Physiol. 2013:**163**(4):1673–1685.
1034 https://doi.org/10.1104/pp.113.224527

1035 **Chen Y, Yu M, Zhang J, Wang X, Shao Q, Yang S, Cao J, Li S, and Liu L**. Multi-omics
1036 integrated analysis reveals the impact of cytokinin on sex differentiation in industrial hemp.
1037 AoB Plants. 2025b:**17**(2). https://doi.org/10.1093/aobpla/plaf019

1038 **Chen Y, Zou T, and McCormick S**. S-adenosylmethionine synthetase 3 is important for pollen
1039 tube growth. Plant Physiol. 2016b:**172**(1):244–253. https://doi.org/10.1104/pp.16.00774

1040 **Cossard GG and Pannell JR**. Enhanced leaky sex expression in response to pollen limitation in
1041 the dioecious plant Mercurialis annua. J Evol Biol. 2021:**34**(2):416–422.
1042 https://doi.org/10.1111/jeb.13720

1043 **Danecek P, Auton A, Abecasis G, Albers CA, Banks E, DePristo MA, Handsaker RE, Lunter**
1044 **G, Marth GT, Sherry ST, et al.** The variant call format and VCFtools. Bioinformatics.
1045 2011:**27**(15):2156–2158. https://doi.org/10.1093/bioinformatics/btr330

1046 **DiMatteo J, Kurtz L, and Lubell-Brand JD**. Pollen appearance and in vitro germination varies
1047 for five strains of female hemp masculinized using silver thiosulfate. HortScience.
1048 2020:**55**(4):547–549. https://doi.org/10.21273/HORTSCI14842-20

1049 **Dowling CA, Shi J, Toth JA, Quade MA, Smart LB, McCabe PF, Schilling S, and Melzer R**.
1050 A FLOWERING LOCUS T ortholog is associated with photoperiod-insensitive flowering in
1051 hemp (Cannabis sativa L.). Plant J. 2024:1–21. https://doi.org/10.1111/tpj.16769

1052 **Eilbeck K, Lewis SE, Mungall CJ, Yandell M, Stein L, Durbin R, and Ashburner M**. The
1053 Sequence Ontology: a tool for the unification of genome annotations. Genome Biol.
1054 2005:**6**(5):1–12. https://doi.org/10.1186/GB-2005-6-5-R44/FIGURES/4

1055 **Emms DM and Kelly S**. OrthoFinder: solving fundamental biases in whole genome comparisons
1056 dramatically improves orthogroup inference accuracy. Genome Biol. 2015:**16**(1):1–14.
1057 https://doi.org/10.1186/s13059-015-0721-2

1058 **Fattel L and Lawrence-Dill CJ**. GO Big or Go Home: A New Gene Ontology Subset that
1059 Improves Plant Gene Function Prediction. bioRxiv. 2025:1–23.
1060 https://doi.org/10.1101/2025.01.26.634938

1061 **Ferfuia C, Zuliani F, Danuso F, Piani B, Cattivello C, Dorigo G, and Baldini M**. Performance
1062 and stability of different monoecious hemp cultivars in a multi-environments trial in north-
1063 eastern Italy. Agronomy. 2021:**11**(7):1–15. https://doi.org/10.3390/agronomy11071424

1064 **Flajšman M, Slapnik M, and Murovec J**. Production of Feminized Seeds of High CBD Cannabis
1065 sativa L. by Manipulation of Sex Expression and Its Application to Breeding. Front Plant Sci.
1066 2021:**12**(November):1–12. https://doi.org/10.3389/fpls.2021.718092

1067 **Galoch E**. The hormonal control of sex differentiation in dioecious plants of hemp (Cannabis
1068 sativa). Acta Soc Bot Pol. 1978:**47**(1–2):153–162.

1069 **García A, Aguado E, Garrido D, Martínez C, and Jamilena M**. Two androecious mutations
1070 reveal the crucial role of ethylene receptors in the initiation of female flower development in
1071 Cucurbita pepo. Plant J. 2020:**103**(4):1548–1560. https://doi.org/10.1111/tpj.14846

1072 **Gaudet P and Dessimoz C**. Gene Ontology: Pitfalls, Biases, and Remedies. . In. C Dessimoz and
1073 N Škunca, eds, Methods in Molecular Biology. (Springer New York: New York, NY), pp.
1074 189–205. https://doi.org/10.1007/978-1-4939-3743-1_14

1075 **Giese MW, Lewis MA, Giese L, and Smith KM**. Development and validation of a reliable and
1076 robust method for the analysis of cannabinoids and terpenes in cannabis. J AOAC Int.
1077 2015:**98**(6):1503–1522. https://doi.org/10.5740/jaoacint.15-116

1078 **Grassa CJ, Weiblen GD, Wenger JP, Dabney C, Poplawski SG, Timothy Motley S, Michael**
1079 **TP, and Schwartz CJ**. A new Cannabis genome assembly associates elevated cannabidiol
1080 (CBD) with hemp introgressed into marijuana. New Phytol. 2021:**230**(4):1665–1679.
1081 https://doi.org/10.1111/nph.17243

1082 **Green G**. The Cannabis Breeder's Bible- The definitive guide to marijuana genetics, cannabis
1083 botany and creating strains for the seed market (Green Candy Press: San Francisco).

1084 **Ji G, Zhang J, Zhang H, Sun H, Gong G, Shi J, Tian S, Guo S, Ren Y, Shen H, et al.** Mutation
1085 in the gene encoding 1-aminocyclopropane-1-carboxylate synthase 4 (CitACS4) led to
1086 andromonoecy in watermelon. J Integr Plant Biol. 2016:**58**(9):762–765.
1087 https://doi.org/10.1111/jipb.12466

1088 **Jones M and Monthony AS**. Cannabis Propagation. . In. Handbook of Cannabis Production in
1089 Controlled Environments. (CRC Press: Boca Raton), pp. 91–121.
1090 https://doi.org/10.1201/9781003150442-4

1091 **Käfer J, Méndez M, and Mousset S**. Labile sex expression in angiosperm species with sex
1092 chromosomes. Philos Trans R Soc B Biol Sci. 2022:**377**(1850).
1093 https://doi.org/10.1098/rstb.2021.0216

1094 **Komai F and Masuda K**. Plasticity in sex expression of spinach (Spinacia oleracea) regenerated
1095 from root tissues. Plant Cell Tissue Organ Cult. 2004:**78**(3):285–287.
1096 https://doi.org/10.1023/B:TICU.0000025665.74491.1e

1097 **Kramer CY**. Extension of Multiple Range Tests to Group Means with Unequal Numbers of
1098 Replications. Biometrics. 1956:**12**(3):307. https://doi.org/10.2307/3001469

1099 **Kurtz LE, Brand MH, and Lubell-Brand JD**. Production of tetraploid and triploid hemp.
1100 HortScience. 2020:**55**(10):1703–1707. https://doi.org/10.21273/HORTSCI15303-20

1101 **Langfelder P and Horvath S**. WGCNA: an R package for weighted correlation network analysis.
1102 BMC Bioinformatics. 2008:**9**(1):559. https://doi.org/10.1186/1471-2105-9-559

1103 **Lapierre É, Monthony AS, and Torkamaneh D**. Genomics-based taxonomy to clarify cannabis
1104 classification. Genome. 2023a. https://doi.org/10.1139/gen-2023-0005

1105 **Lapierre É, de Ronne M, Boulanger R, and Torkamaneh D**. Comprehensive Phenotypic
1106 Characterization of Diverse Drug-Type Cannabis Varieties from the Canadian Legal Market.
1107 Plants. 2023b:**12**(21):1–17. https://doi.org/10.3390/plants12213756

1108 **Li H**. Aligning sequence reads, clone sequences and assembly contigs with BWA-MEM. 2013.

1109 **Li Q, Guo W, Chen B, Pan F, Yang H, Zhou J, Wang G, and Li X**. Transcriptional and
1110 Hormonal Responses in Ethephon-Induced Promotion of Femaleness in Pumpkin. Front Plant
1111 Sci. 2021:**12**(1). https://doi.org/10.3389/fpls.2021.715487

1112 **Lin H, Liao Z, Zhang L, and Yu Q**. Transcriptome analysis of the male-to-hermaphrodite sex
1113 reversal induced by low temperature in papaya. Tree Genet Genomes. 2016:**12**(5).
1114 https://doi.org/10.1007/s11295-016-1055-2

1115 **Love MI, Huber W, and Anders S**. Moderated estimation of fold change and dispersion for
1116 RNA-seq data with DESeq2. Genome Biol. 2014:**15**(12):1–21.
1117 https://doi.org/10.1186/s13059-014-0550-8

1118 **Lubell JD and Brand MH**. Foliar sprays of silver thiosulfate produce male flowers on female
1119 hemp plants. Horttechnology. 2018:**28**(6):743–747.

https://doi.org/10.21273/HORTTECH04188-18

McDonald JH. Handbook of Biological Statistics 3rd ed. (Sparky House Publishing: Baltimore).

McLaren W, Gil L, Hunt SE, Riat HS, Ritchie GRS, Thormann A, Flicek P, and Cunningham F. The Ensembl Variant Effect Predictor. Genome Biol. 2016:**17**(1):1–14. https://doi.org/10.1186/s13059-016-0974-4

Monthony AS, Bagheri S, Zheng Y, and Jones AMP. Flower power: floral reversion as a viable alternative to nodal micropropagation in Cannabis sativa. Vitr Cell Dev Biol - Plant. 2021a:**21**:1–13. https://doi.org/10.1007/s11627-021-10181-5

Monthony AS, Page SR, Hesami M, and Jones AMP. The Past, Present and Future of *Cannabis sativa* Tissue Culture. Plants. 2021b:**10**(1):185. https://doi.org/10.3390/plants10010185

Monthony AS, de Ronne M, and Torkamaneh D. Exploring ethylene-related genes in Cannabis sativa: implications for sexual plasticity. Plant Reprod. 2024. https://doi.org/10.1007/s00497-023-00492-5

Moon Y-H, Lee YJ, Koo SC, Hur M, Huh YC, Chang J-K, and Park WT. Effect of Timing of Ethephon Treatment on the Formation of Female Flowers and Seeds from Male Plant of Hemp (Cannabis sativa L.). Plant Resour Soc Korea. 2020:**33(6)**(6):682–688. https://doi.org/10.7732/KJPR.2020.33.6.682

Mudge EM, Brown PN, and Murch SJ. The Terroir of *Cannabis*: Terpene Metabolomics as a Tool to Understand *Cannabis sativa* Selections. Planta Med. 2019:**85**(9–10):781–796. https://doi.org/10.1055/a-0915-2550

NCBI. Cannabis sativa "Pink Pepper" genome assembly GCA_029168945.1/ASM2916894v1. 2023.

Nei M and Li WH. Mathematical model for studying genetic variation in terms of restriction endonucleases. Proc Natl Acad Sci. 1979:**76**(10):5269–5273. https://doi.org/10.1073/PNAS.76.10.5269

Orozco LR, Weaver AE, Pauli CC, Grassa CJ, Vergara D, Baptista A, White K, Emery BF, Castro NRM, Guerrero RF, et al. Unraveling Cross-Cellular Communication in Cannabis sativa Sex Determination: A Network Ontology Transcript Annotation (Nota) Analysis. 2025. https://doi.org/10.1101/2025.05.05.650505

Page SRG, Monthony AS, and Jones AMP. DKW basal salts improve micropropagation and callogenesis compared with MS basal salts in multiple commercial cultivars of Cannabis sativa. Botany. 2021:**99**(5):269–279. https://doi.org/10.1139/cjb-2020-0179

Piepho HP. An algorithm for a letter-based representation of all-pairwise comparisons. J Comput Graph Stat. 2004:**13**(2):456–466. https://doi.org/10.1198/1061860043515

van de Poel B, Bulens I, Markoula A, Hertog MLATM, Dreesen R, Wirtz M, Vandoninck S, Oppermann Y, Keulemans J, Hell R, et al. Targeted systems biology profiling of tomato fruit reveals coordination of the Yang cycle and a distinct regulation of ethylene biosynthesis during postclimacteric ripening. Plant Physiol. 2012:**160**(3):1498–1514. https://doi.org/10.1104/pp.112.206086

1159 **Van de Poel B, Vandenzavel N, Smet C, Nicolay T, Bulens I, Mellidou I, Vandoninck S,**
1160 **Hertog MLATM, Derua R, Spaepen S, et al.** Tissue specific analysis reveals a differential
1161 organization and regulation of both ethylene biosynthesis and E8 during climacteric ripening
1162 of tomato. BMC Plant Biol. 2014:**14**(1). https://doi.org/10.1186/1471-2229-14-11

1163 **Pommerrenig B, Feussner K, Zierer W, Rabinovych V, Klebl F, Feussner I, and Sauera N**.
1164 Phloem-Specific expression of Yang cycle genes and identification of novel Yang cycle
1165 enzymes in Plantago and Arabidopsis. Plant Cell. 2011:**23**(5):1904–1919.
1166 https://doi.org/10.1105/tpc.110.079657

1167 **Prentout D, Razumova O, Rhoné B, Badouin H, Henri H, Feng C, Käfer J, Karlov G, and**
1168 **Marais GAB**. An efficient RNA-seq-based segregation analysis identifies the sex
1169 chromosomes of Cannabis sativa. Genome Res. 2020:**30**(2):164–172.
1170 https://doi.org/10.1101/gr.251207.119

1171 **Punja ZK and Holmes JE**. Hermaphroditism in Marijuana (Cannabis sativa L.) Inflorescences –
1172 Impact on Floral Morphology, Seed Formation, Progeny Sex Ratios, and Genetic Variation.
1173 Front Plant Sci. 2020:**11**(June):1–20. https://doi.org/20

1174 **Putri GH, Anders S, Pyl PT, Pimanda JE, and Zanini F**. Analysing high-throughput sequencing
1175 data in Python with HTSeq 2.0. Bioinformatics. 2022:**38**(10):2943–2945.
1176 https://doi.org/10.1093/bioinformatics/btac166

1177 **Quinlan AR and Hall IM**. BEDTools: a flexible suite of utilities for comparing genomic features.
1178 Bioinformatics. 2010:**26**(6):841–842. https://doi.org/10.1093/BIOINFORMATICS/BTQ033

1179 **Rajagopalan PA, Saraf-Levy T, Lizhe A, and Perlp-Treves R**. Increased femaleness in
1180 transgenic cucumbers that over-express an ethylene receptor. . In. Progress in cucurbit
1181 genetics and breeding research. Proceedings of Cucurbitaceae 2004, the 8th EUCARPIA
1182 meeting on Cucurbit Gentics and Breeding, A Lebeda and HS Paris, eds. (Olomouc), pp. 525–
1183 531.

1184 **Ram HYM and Jaiswal VS**. Induction of female flowers on male plants of Cannabis Sativa L.
1185 by 2-chloroethanephos-phonic acid. Experientia. 1970:**26**(2):214–216.
1186 https://doi.org/10.1007/BF01895593

1187 **Rau A, Gallopin M, Celeux G, and Jaffrézic F**. Data-based filtering for replicated high-
1188 throughput transcriptome sequencing experiments. Bioinformatics. 2013:**29**(17):2146–2152.
1189 https://doi.org/10.1093/bioinformatics/btt350

1190 **Reed J**. Morphology of *Cannabis sativa* L. 1914. https://doi.org/10.17077/etd.jn36uz6v

1191 **Resnick JS, Wen C-KCK, Shockey JA, and Chang C**. REVERSION-TO-ETHYLENE
1192 SENSITIVITY1, a conserved gene that regulates ethylene receptor function in Arabidopsis.
1193 Proc Natl Acad Sci. 2006:**103**(20):7917–7922. https://doi.org/10.1073/pnas.0602239103

1194 **Roy J, Monthony AS, and Torkamaneh D**. DESeq2-MultiBatch: Batch Correction for Multi-
1195 Factorial RNA-seq Experiments. bioRxiv. 2025. https://doi.org/10.1101/2025.04.20.649392

1196 **Rzewuski G, Cornell KA, Rooney L, Bürstenbinder K, Wirtz M, Hell R, and Sauter M**.
1197 OsMTN encodes a 5′-methylthioadenosine nucleosidase that is up-regulated during
1198 submergence-induced ethylene synthesis in rice (Oryza sativa L.). J Exp Bot.

2007:**58**(6):1505–1514. https://doi.org/10.1093/jxb/erm014

Sather DN, Jovanovic M, and Golenberg EM. Functional analysis of B and C class floral organ genes in spinach demonstrates their role in sexual dimorphism. BMC Plant Biol. 2010:**10**. https://doi.org/10.1186/1471-2229-10-46

Shi J, Schilling S, and Melzer R. Morphological and genetic analysis of inflorescence and flower development in hemp (Cannabis sativa L .). bioRxiv. 2024a. https://doi.org/https://doi.org/10.1101/2024.01.25.577276

Shi J, Toscani M, Dowling CA, Schilling S, and Melzer R. Identification of genes associated with sex expression and sex determination in hemp (Cannabis sativa L.). bioRxiv. 2024b.

Solano R, Stepanova A, Chao Q, and Ecker JR. Nuclear events in ethylene signaling: A transcriptional cascade mediated by ETHYLENE-INSENSITIVE3 and ETHYLENE-RESPONSE-FACTOR1. Genes Dev. 1998:**12**(23):3703–3714. https://doi.org/10.1101/gad.12.23.3703

Spitzer-Rimon B, Duchin S, Bernstein N, and Kamenetsky R. Architecture and florogenesis in female *Cannabis sativa* plants. Front Plant Sci. 2019:**10**(April 2019):1–11. https://doi.org/10.3389/fpls.2019.00350

Stephens M. False discovery rates: A new deal. Biostatistics. 2017:**18**(2):275–294. https://doi.org/10.1093/biostatistics/kxw041

Thomas TD. In vitro modification of sex expression in mulberry (Morus alba) by ethrel and silver nitrate. Plant Cell Tissue Organ Cult. 2004:**77**(3):277–281. https://doi.org/10.1023/B:TICU.0000018390.65934.93

Tian J, Zhang F, Zhang G, Li X, Wen C, and Li H. A long noncoding RNA functions in pumpkin fruit development through S -adenosyl- L -methionine synthetase. Plant Physiol. 2024:**195**(2):940–957. https://doi.org/10.1093/plphys/kiae099

Torkamaneh D, Laroche J, Tardivel A, O'Donoughue L, Cober E, Rajcan I, and Belzile F. Comprehensive description of genomewide nucleotide and structural variation in short-season soya bean. Plant Biotechnol J. 2018:**16**(3):749–759. https://doi.org/10.1111/pbi.12825

Toth JA. Elucidating the genetic control of qualitative traits in hemp. 2022.

Toth JA, Stack GM, Cala AR, Carlson CH, Wilk RL, Crawford JL, Viands DR, Philippe G, Smart CD, Rose JKC, et al. Development and validation of genetic markers for sex and cannabinoid chemotype in Cannabis sativa L. GCB Bioenergy. 2020:**12**(3):213–222. https://doi.org/10.1111/gcbb.12667

Tsuji H. Molecular function of florigen. Breed Sci. 2017:**67**(4):327–332. https://doi.org/10.1270/jsbbs.17026

Uygun S, Peng C, Lehti-Shiu MD, Last RL, and Shiu SH. Utility and Limitations of Using Gene Expression Data to Identify Functional Associations. PLoS Comput Biol. 2016:**12**(12):1–27. https://doi.org/10.1371/journal.pcbi.1005244

Waduwara-Jayabahu I, Oppermann Y, Wirtz M, Hull ZT, Schoor S, Plotnikov AN, Hell R,

1237 **Sauter M, and Moffatt BA**. Recycling of methylthioadenosine is essential for normal
1238 vascular development and reproduction in Arabidopsis. Plant Physiol. 2012:**158**(4):1728–
1239 1744. https://doi.org/10.1104/pp.111.191072

1240 **Wang Q, Zeng X, Song Q, Sun Y, Feng Y, and Lai Y**. Identification of key genes and modules
1241 in response to Cadmium stress in different rice varieties and stem nodes by weighted gene
1242 co-expression network analysis. Sci Rep. 2020:**10**(1):9525. https://doi.org/10.1038/s41598-
1243 020-66132-4

1244 **Waters Corporation**. Waters Kairos Amino Acid Kit (Milford).

1245 **Welling MT, Deseo MA, Bacic A, and Doblin MS**. Untargeted Metabolomic Analyses Reveal
1246 Chemical Complexity of Dioecious Cannabis Flowers. Aust J Chem. 2021:**74**(6):463–479.
1247 https://doi.org/10.1071/CH21033

1248 **Wickham H**. ggplot2: Elegant Graphics for Data Analysis 1st ed. (Springer New York: New York,
1249 NY). https://doi.org/10.1007/978-0-387-98141-3

1250 **Zhang J, Shi J, Ji G, Zhang H, Gong G, Guo S, Ren Y, Fan J, Tian S, and Xu Y**. Modulation
1251 of Sex Expression in Four Forms of Watermelon by Gibberellin, Ethephone and Silver
1252 Nitrate. Hortic Plant J. 2017:**3**(3):91–100. https://doi.org/10.1016/j.hpj.2017.07.010

1253 **Zheng Y**. Handbook of Cannabis Production in Controlled Environments First Edit. Y Zheng, ed
1254 (CRC Press: Boca Raton). https://doi.org/10.1201/9781003150442

1255

Supplementary Table Captions

Supplementary Table 1 Cutting, vegetative and flowering growth conditions. Following rooting of cuttings, all plants were grown in controlled growth chambers. Male flowers (MF); female flowers (FF); induced female flowers (IFF); induced male flowers (IMF); as needed (PRN), Photosynthetic Photon Flux Density (PPFD).

Supplementary Table 2 Primer sequences used for sexing in a PACE assay, table extracted from Toth (2022).

Supplementary Table 3 Cannabinoid standards used in the cannabinoid quantification by UPLC-PDA. All standards were purchased from Agilent.

Supplementary Table 4 ACC and SAM working solutions (WS) and calibration standards (C) concentrations before/after derivatization with AccQ-Tag.

Supplementary Table 5 UPLC Gradient Elution Program Adapted from Kairos et al. (2019). The table outlines the gradient conditions used for chromatographic separation of ACC and SAM. Mobile phase A consists of 0.1% formic acid in water, while mobile phase B consists of 0.1% formic acid in acetonitrile.

Supplementary Table 6 Optimized Xevo TQ-S Mass Spectrometry Parameters for ACC and SAM Analysis.

Supplementary Table 7 Multiple Reaction Monitoring (MRM) Transitions for ACC and SAM Detection. m/z: refers to the mass-to-charge ratio of the ions detected; sd: denotes single dissociation, indicating that the precursor ion undergoes a single-step fragmentation before detection.

Supplementary Table 8 Metadata and RNA-seq quality control metrics for samples included in this study. Columns include sample name, genotype, genetic sex, tissue type, sample timepoint, treatment (Ctrl = control; ET = ethephon; STS = Silver thiosulfate), RNA integrity number (RIN) following sample RNA extraction, sequencing depth (coverage, ×), GC content (%), and average mapping quality following alignment with STAR and post-alignment QC using Qualimap. The final two columns indicate whether each sample passed internal quality filters and was retained for downstream weighted gene co-expression network analysis (WGCNA) and differential expression analysis (DESeq2), respectively.

1292

1293 **Supplementary Table 9** Results of the F-test from the ANOVA for the percentage of *C. sativa*
1294 florets which underwent sex change.

1295

1296 **Supplementary Table 10** Cannabinoid content (% w/w) of mature female flowers for the
1297 genotypes used in the present study and the analytical limit of quantification (LOQ) and limit of
1298 detection (LOD) for the cannbinoids analyzed. ND indicates that the sample was below the limit
1299 of detection. The cannabinoid abbreviations are as follows: tetrahydrocannabinolic acid (THCA),
1300 delta-9-tetrahydrocannabinol (Δ9-THC), cannabidiolic acid (CBDA), cannabidiol (CBD),
1301 cannabigerolic acid (CBGA), cannabigerol (CBG), cannabichromene (CBC), cannabinol (CBN),
1302 tetrahydrocannabivarin (THCV), and cannabidivarin (CBDV).

1303

1304 **Supplementary Table 11** *C. sativa* ERGs as identified through homology analysis using the
1305 current reference genome ('Pink Pepper'; NCBI, 2023), X and Y haplotypes from the Otto II
1306 genotype, and the previous reference genome, Cs10 (Grassa et al. 2021). Chr: chromosome
1307 number.

1308

1309 **Supplementary Table 12** Genetic diversity analysis of XX and XY genotypes Deadly Kernel,
1310 La Rosca and Panama Pupil V4.

1311

1312 **Supplementary Table 13** Quantification data (ug/g fresh weight) of 1-aminocyclopropane-1-
1313 carboxylic acid (ACC) and detection of S-adenosylmethionine (SAM) by UPLC-MS.

1314

1315 **Supplementary Table 14** ERGs identified within treatment-associated modules from the XX and
1316 XY network before differential gene expression filtering. Module-trait correlations (r) indicate the
1317 relationship between each module and treatment (STS for XX and ethephon for XY) or time points
1318 (Day 1 and Day 14). Intramodular connectivity (kME) reflects the centrality of each gene within
1319 its assigned module.

1320

1321 # Supplementary Figures Captions

Supplemental Figure 1 Representative timeline of floral development in MF, IMF, FF and IFF of *C. sativa* 'Deadly Kernel' (DK) and 'Panama Pupil V4' (PP) from 7 to 28 days after the photoperiod shift from long day to short day. N/A indicates photo not available for a given time/treatment.

1322

Supplemental Figure 2 Differential expression data contrasting control (MF or FF) and sex changed (IFF or IMF) plants at day 1 and 14 using the 24 ERGs identified from WGCNA. Genes which show genotype-independent behaviour (gray highlight) were retained for further analysis.

1323

Supplemental Figure 3 Genomic distribution and predicted impact of SNPs and structural variants (SVs) in the 47 ERGs of the six C. sativa samples. A) Schematic representation of a gene structure and its surrounding regulatory regions (5 kb upstream and downstream), highlighting genomic elements considered in the analysis. Regions are color-coded based on their predicted impact, ranging from modifier (low impact, mostly regulatory) to low, moderate, or high impact (potential functional consequences protein function). Distribution of SNPs (B) and SVs (C) categorized by their predicted impact and localization. D) Distribution of modifier impact variants (SNPs and SVs) across the 47 ERGs. E) Distribution of low to high impact variants identified in the 47 ERGs.

1324

Supplemental Figure 4 Endogenous ACC concentrations and their correlation with CsCTR1-LIKE expression in C. sativa leaves during floral transition. A) ACC quantification at vegetative (day 0) and flowering (day 1) stages across experimental groups. Error bars represent standard error of the estimated marginal means. Different letters indicate significant differences among groups (Tukey's HSD, $\alpha = 0.05$). B) Spearman correlation heatmap depicting the relationship between CsCTR1-LIKE (LOC115706236) expression and ACC concentration across treatment groups. A significant negative correlation ($\rho = -0.8$, $p \leq 0.001$) is observed in XX Day 0 – FF. Statistical significance for Spearman correlations was categorized as follows: $p \leq 0.001$, ***; $p \leq 0.01$, **; $p \leq 0.05$, *; correlations with $p > 0.05$ were considered non-significant.

1325

Supplemental Figure 5 WGCNA module identification and correlation analysis. A, B) Clustering dendrogram for XX (A) and XY (B) plants. C-D) Module-trait correlation heatmaps of identified modules correlated with treatment and day. Modules significantly associated with the traits with identified with $|cor| > 0.5$ and p value ≤ 0.05, and are indicated by asterisks as follows: $p \leq 0.001$, ***; $p \leq 0.01$, **; $p \leq 0.05$, *; correlations with $p > 0.05$ were considered non-significant. Red and blue color notes positive and negative correlation between a given module and trait pair.

1326